Spring 4-2016

The ~860 Ma mafic dikes and granitoids from the northern margin ofthe Yangtze Block, China: A record of oceanic subduction in the earlyNeoproterozoic

Ali Polat
University of Windsor

The ~860 Ma mafic dikes and granitoids from the northern margin of the Yangtze Block, China: A record of oceanic subduction in the early Neoproterozoic

Yang Xu[a, b, c, d], Kun-Guang Yang*[a, d], Ali Polat[e,f], Zhen-Ning Yang[a, d]

[a]School of Earth Sciences, China University of Geosciences Wuhan, Wuhan 430074, China

[b]Qingdao Institute of Marine Geology, Qingdao 266071, China

[c]Key Laboratory of Marine Hydrocarbon Resources and Environmental Geology, Ministry of Land and Resources, Qingdao 266071, China

[d]Key Laboratory of Tectonics and Petroleum Resources, Ministry of Education, China University of Geosciences Wuhan, Wuhan 430074, China

[e]University of Windsor, Department of Earth and Environmental Sciences, University of Windsor, Windsor, ON, Canada N9B 3P4

[f]Center for Global Tectonics, School of Earth Sciences, China University of Geosciences, Wuhan, 430074

ABSTRACT

There are voluminous Neoproterozoic arc-related volcano-sedimentary sequences and small intrusions on the northern margin of the Yangtze Block, South China. The understanding the origin of the Sanligang granitoid intrusion and the spatially associated mafic dikes in the region is crucial for unravelling the tectonic evolution and continental crust growth processes in the Yangtze Block. Zircon U-Pb dating suggests that the mafic dikes (ca. 870 Ma) and granitoids (860 Ma) are contemporaneous. The mafic dikes have low SiO_2 (45.37–46.55 wt.%), K_2O (0.32–0.82 wt.%) and Na_2O (2.01–2.85 wt.%), and are characterized by enrichment in large ion lithophile elements (LILEs) and depletion in

Correponding Author: Kungang Yang
Address: No.388, Lumo Road, Wuhan City, Hubei Province, China
Tel: +86 27 67883596
Email: yangkunguang@163.com

high-field strength elements (HFSEs), suggesting that their mantle source was modified by subducted materials. The Sanligang granitoids have intermediate to high SiO_2 (60.35–71.38 wt.%), intermediate K_2O (1.38–3.67 wt.%) and Na_2O (3.97–5.33 wt.%), and high MgO (1.03–3.16 wt.%). They show LREE-enriched REE patterns (La/Yb_N = 7.2–12.3) with no or minor negative Eu anomalies. Their primitive mantle-normalized trace element patterns are characterized by enrichment of LILEs and depletion of HFSEs. Both the mafic dikes and granitoids share similar zircon $\varepsilon_{Hf}(t)$ values (+10.5 to +12.9, +7.9 to +11.7, respectively), whole-rock initial $^{87}Sr/^{86}Sr$ ratios (0.7051–0.7057, 0.7033–0.7041, respectively) and $\varepsilon_{Nd}(t)$ values (+4.0 to +7.1, +3.4 to +4.9, respectively), suggesting that the granitoids were generated by partial melting of juvenile basaltic crust. High Mg# values (49-58) in the granitoids may have resulted from assimilation of residual mafic minerals in their source region. Based on its arc-related geochemical affinity and contemporaneous arc-related magmatism, the Sanligang pluton is proposed to be generated in a Neoproterozoic arc setting during crustal growth and reworking. The early Neoproterozoic assemblage from the Sangligang-Sanyang fault belt provides an important record of oceanic slab subduction in the northern margin of the Yangtze Block.

Keywords: Zircon geochronology; Zircon Hf isotope; Arc-related intrusion; Neoproterozoic tectonics; Northern margin of the Yangtze Block

1. Introduction

Worldwide occurrences of late Mesoproterozoic to early Neoproterozoic magmatic rocks indicate major episodes of crustal growth and tectonic events in the Proterozoic (Li et al., 1995; 2003c; 2008). The South China Block is considered to have been involved in the assembly and breakup of the supercontinent Rodinia (Li et al., 2003a; 2003c; 2008). Late Mesoproterozoic to early Neoproterozoic igneous rocks are also widespread around the Yangtze Block (e.g., Zhou et al., 2002, 2006; Ling et al., 2003; Geng et al., 2008; Dong et al., 2012; Du et al., 2014; Charvet, 2013; Wang and Zhou, 2012; Wang et al., 2013; Zhao et al., 2010b; 2013a; 2013b; Qiu et al., 2011; Peng et al., 2012). Understanding the origin of these rocks is important for constraining crustal growth and tectonic reworking events in the Yangtze Block and surrounding region, as well as reconstruction of the supercontinent Rodinia (Wang et al., 2009; Zhao et al, 2012; Zhang et al, 2013a; 2013b; 2013c; Chen et al., 2014).

South China comprises the Yangtze Block to the west and the Cathaysia Block to the east that were previously considered to have been amalgamated at the end of the Mesoproterozoic associated with the assembly of Rodinia, and occupied an intracratonic keystone position between Australia and Laurentia (e.g., Li et al., 1995; 2008). However, this model is not consistent with the presence of the Neoproterozoic (970–900 Ma) arc–affinity igneous rocks around the Yangtze Block (e.g., Cawood et al., 2013; Charvet, 2013; Wang et al., 2013). New geochronological and geochemical data suggest that the final stage of the assemblage of the Yangtze and Cathaysia blocks was completed at approximately 820 Ma (Zhao et al., 2011; Zhang et al., 2012; 2013a; 2013c; 2015). Thus，the Yangtze Block was located at the margin of Rodinia or external to the supercontinent (e.g., Zhou et al., 2006; Wang and Zhou, 2012; Wang et al., 2013; Du et al., 2014).

Many models have been proposed for the formation of the Neoproterozoic igneous rocks in the Yangtze Block; these models include the “slab-arc model” (Zhou et al., 2002, 2006; Zhao and Zhou, 2007; 2008; Zhao et al., 2010a; 2010b; 2013a; 2013b), “plume-rift model” (Li et al., 2002; 2003a; 2003b; 2003c; Wang et al., 2009) and “plate-rift model” (Zheng et al., 2007, 2008; Huang et al., 2009). The “rift” and “plume” models suggest that the 850–750 Ma igneous rocks formed in an extensional tectonic environment related to breakup of Rodinia, whereas the “arc” model considers that these rocks were formed in continental arc settings. It was a debated issue whether the 850 to 750 Ma arc-affinity rocks were formed in arc settings or derived from the pre-existing juvenile arc crustal rocks under an anorogenic setting (e.g., Li et al., 2003a; 2003b; Huang et al.; 2009; Wang et al., 2009).

The Neoproterozoic igneous rocks from the northern margin of the Yangtze Block are rarely investigated (Zhao and Cawood, 2012; Bader et al., 2013; Zhang et al., 2013a). Comprehensive geochronological and geochemical studies are necessary for understanding the place of the Yangtze Block in Rodinia. Some Neoproterozic mafic rocks and granitoids were recently identified in the Sanligang–Sanyang fault belt (SSFB) at the northern margin of the Yangze Block (Dong et al., 1999; 2004; Lai et al., 2004; Shi et al., 2003; 2005; 2007). However, lithological assemblages, ages, and tectonic settings of these rocks are still unclear. The Sanligang pluton is the only granitoid body identified in the region and thus provides a good opportunity to understand the Neoproterozoic petrogenetic and geodynamic processes took place the region. In this paper, we present new zircon U–Pb ages, Hf isotopes, and whole-rock elemental and isotopic data. These data demonstrate that the Sanligang mafic dikes and granitic pluton formed in the early Neoproterozoic, recording the Proterozoic arc magmatism resulting from oceanic slab subduction beneath the northern margin of the

Yangtze Block.

2. Geological background and sample description

South China is tectonically composed of two major blocks, namely, Yangtze to the northwest and Cathaysia to the southeast (Fig.1a). These blocks were assumed to be amalgamated during the Jiangnan orogeny between 850 and 830 Ma (Zhang et al., 2013a). The Yangtze Block is separated from the South Qinling-Tongbai orogen to its north by the Triassic Mianlue suture zone (MLSZ) and the Xiang–Guang faults (XGF) and from the Songpan and Bikou terranes to its west by the Longmenshan orogen (Fig.1b). The Yangtze Block consists of highly metamorphosed Neoarchean to Paleoproterozoic crystalline basement rocks, Mesoproterozoic to Neoproterozoic greenschist facies transitional basement rocks, and non-metamorphosed Sinian–Mesozoic clastic and carbonate sedimentary cover sequence (Zhao and Cawood, 2012).

The Tongbai orogen, which is the eastward extension of the South Qinling orogen, marks the Permo–Triassic collision zone between the North China Craton and the Yangtze Block (e.g., Zhang et al., 2004). The orogen can be generally separated into two parts by the Xin–Huang fault: the Tongbai UHP complex to the north and the Suizhou greenschist assemblage to the south (Fig.1b). The Tongbai UHP complex consists of granitic gneisses with subordinate amphibolites and metasedimentary rocks that are characterized by UHP eclogites overprinted by granulite/amphibolite retrograde metamorphism. The Suizhou greenschist assemblage is composed of basement complexes and overlain by the Neoproterozoic to Mesozoic sedimentary cover. The basement complexes are mainly composed of the Neoproterozoic Wudang and Yaolinghe Groups, both of which are characterized by rift-related greenschist facies meta-igneous rocks (Ling et al., 2008). The Wudang and Yaolinghe Groups are unconformably overlain by the unmetamorphosed Neoproterozoic Sinian sedimentary sequence.

The most important tectonic boundary is the XGF that separates the Tongbai orogen to the north from the Yangtze Block to the south. The XGF is also the most important decollement surface by which the Tongbai Block thrust toward the south following the Triassic collision (Dong et al., 2005). The tectonic settings and genetic mechanism of XGF remain controversial, and one of the most widely accepted views is that XGF is an ophiolitic tectonic mélange that represents the vestiges of the easternmost MLSZ (Dong et al., 2004; Shi et al., 2005; Zhang et al., 2004).

The Sanligang-Sanyang region, along the west sector of XGF (ca.100 km long and 1–5 km wide) is the best representative area of the tectonic mélange belt and the eastward extension of MLSZ (Dong et al., 2003; 2004; Lai et al., 2004). The northwest-striking SSFB is composed of different tectonic blocks with different lithological characteristics and ages, which mainly include ophiolitic fragments, island-arc volcanic rocks, slices of pelagic sedimentary andfore-arc volcano–sedimentary rocks, crystalline basement rocks and overlying cover strata of the Yangtze Block. These blocks are separated by by shear zones and dispersed in deformed matrix composed of the fore-arc volcaniclastic and pelagic sedimentary rocks (Dong et al., 1999). Moreover, the NW–SE trending Sanligang dioritic to granodioritic pluton is exposed along the SSFB (Fig.1c).

The ophiolitic and island-arc volcanic blocks are principally composed of gabbro, diabase, basalt and andesite, which were separated from the Huashan Group in the Sanligang area. The geochemical characteristics of these rocks reveal that they formed in an island-arc or in an initial oceanic basin setting (Dong et al., 2004). Dong et al. (2004) and Lai et al. (2004) used strata correlation to propose that the Sanligang–Sanyang tectonic mélange belt formed in the Neopaleozoic–Early Triassic and represents the eastern part of the Mianlüe ophiolitic mélange. Recent SHRIMP zircon U-Pb dating of gabbros from these ophiolitic blocks indicates that they formed in the Neoproterozoic (947 ± 14 Ma) (Shi et al., 2007). Other, older volcanic and sedimentary sequences are not recognized. These results have led geologists to focus on the study of the early Neoproterozoic geologic record in the SSFB (Bader et al., 2013).

The Neoproterozoic Huashan Group in the SSFB constitutes the Precambrian basement of the Yangtze Block. It has an unconformable contact with the underlying Mesoproterozoic Dagushi Group, and is unconformably overlain by the Sinian sequence, which consists from bottom to top of conglomerate, sandstone, siltstone, mudstone, mud-slate, and mafic volcanic rocks. The cover sequence of the Yangtze Block is composed mainly of Neoproterozoic Sinian–Palaeozoic clastic and carbonate sedimentary rocks.

2.1. Mafic dikes

Mafic rocks in the SSFB are distributed mainly in theTumen, Sanligang, Zhoujiawan and Xiaofu areas. The mafic rocks in the Sanligang area include mainly basalts with minor gabbros and diabase dikes. No ultramafic rocks have been found in this region so far. The diabase dikes and gabbros generally intrude basalts or are tectonically emplaced in the Huashan Group (Fig. 1c). The gabbros diabase dikes are spatially associated in the field..

The mafic dikes outcrop in Yangjiapeng village ca. 4 km south of Sanligang town (Fig. 1c). The lithological, geochemical, and geochronologic characteristics of these rocks are reported by Shi et al. (2005; 2007). Recently, several outcrops of mafic dikes were found during mining and housing construction in the vicinity of Sanligang (Figs. 1c and 2a). One of mafic dikes was intruded by granitoid and preserved as a lensoidal enclave in the Sanligang grantic pluton. This enclave is dark green and has a massive structure. Major minerals include plagioclase (45–55%), hornblende (20–25%), augite (10–20%) and magnetite (1–2%) (Fig. 3a). The grain size of augite is generally 0.2–2 mm. Many grains were altered to amphibole and chlorite, only a few original grains remained. Euhedral plagioclase laths are typically 0.5–2 mm in size. The plagioclase grains are altered to clay minerals. Amphibole occurs mainly as alteration product of pyroxene. The relevant petrographical features are given in Table 1.

2.2. Granitoid pluton

The Sanligang granitic pluton is located ca. 300–400 m west of Sanligang and crops out over approximately 7–8 km^2. It intrudes the sedimentary rocks of the Huashan Group, basalts and mafic dikes in the west and south, and is in a tectonic contact with the Sinian to Cambrian sequence in the east (Figs. 1, 2b and 2c). The Sanligang granitic pluton was considered as a Mesozoic pluton (HBBGMR, 1982). However, SHRIMP zircon U–Pb dating has recently demonstrated that the emplacement age of the Sanligang pluton is 876 ± 7 Ma (Shi et al., 2007).

The Sanligang granitic pluton is dominated by quartz diorite and granodiorite. Quartz diorite is light dark and medium grained with a massive structure; it consists of plagioclase (55–60%), hornblende (10–20%), and quartz (10–20%), with minor K-feldspar (Table 1, Figs. 2d, 3b). The granodiorite contains plagioclase (40–60%), quartz (20–35%), and hornblende (5–15%), with minor biotite and K-feldspar; it also has a medium-grained phaneritic texture and a massive appearance (Table 1, Figs. 2c, 3c and 3d). Most plagioclase grains occur as euhedral granular crystals and show typical mosaic textures with other minerals. Moreover, all samples were variably altered, with amphibole being replaced by chlorite and/or epidote (Fig. 3d) and feldspar altered typically to sericite and kaolinite. Folds, deformation lamellae in plagioclase, curved joint of hornblende, and undulatory extinction quartz show that the pluton has experienced compressional deformation (Figs. 3e and 3f). A few of pelitic xenoliths and mafic enclaves are observed in the pluton, especially at the margins, and most of them have sharp, well-defined contacts with the host rock (Figs. 2e and 2f). The detailed petrographic features are presented in Table 1.

3. Analytical methods

3.1 Zircon U–Pb dating analysis

Uranium, Th and Pb isotopic measurements of samples S07 and S31 were conducted at the Institute of Geology and Geophysics, Chinese Academy of Sciences, Beijing, using the Cameca IMS-1280 SIMS. Uranium–Th–Pb isotopic ratios and absolute element abundances were determined relative to the standard zircon Plešovice (Sláma et al., 2008) and 91500 (Wiedenbeck et al., 1995), respectively, using operating and data processing procedures described by Li et al. (2009). Uncertainties on individual analysis in the data tables are reported at the 1σ level. The weighted mean U–Pb ages and Concordia plots were processed using Isoplot/Ex v.3.0 (Ludwig, 2003). The SIMS zircon U–Pb isotopic data are reported in Table 2.

The LA–ICP–MS U–Pb dating of samples S04 and S10 was conducted using an Agilent 7500a ICP–MS with an attached 193 nm excimer ArF laser–ablation system at the State Key Laboratory of Geological Processes and Mineral Resources, China University of Geosciences, Wuhan (SKLGPMR-CUG). The detailed analytical procedures are described by Liu et al. (2008). All measurements were performed using zircon 91500 as the reference standard with a recommended $^{206}Pb/^{238}U$ age of 1065.4 ± 0.6 Ma. Common Pb correction was made using the EXCEL spreadsheet ComPbCorr#3_151 (Andersen, 2002). Off-line selection and integration of analyte signals, as well as mass bias calibrations were performed using ICPMSDataCal (Liu et al., 2010). The results are listed in Table 2.

3.2 Zircon Lu–Hf isotope analysis

In situ zircon Lu-Hf isotopic measurements of samples S04, S07, S10 and S31 were performed at the SKLGPMR-CUG. The measurements were obtained using a Neptune multi-collector ICP–MS equipped with a Geolas-193 Geolas 2005 excimer ArF laser ablation system. Detailed analytical procedures are given by Hu et al. (2012). Measured $^{176}Hf/^{177}Hf$ ratios were normalized to $^{179}Hf/^{177}Hf$ = 0.7325. Further external adjustment was not applied for the unknowns because our determined $^{176}Hf/^{177}Hf$ ratios for zircon standards 91500 (0.282308 ± 0.000004) and GJ-1 (0.282021 ± 0.000011) agreed within the errors of the reported values (Griffin et al., 2006). The zircon Hf isotopic data are presented in Table 3.

3.3. Whole–rock major and trace element analyses

Major element oxides and trace elements were analyzed using a Magix-pro2440 fluorescence spectrometer and a Thermoel Emental X7 ICP–MS instrument, respectively, at the Wuhan Testing Center of Mineral Resources Supervision, Ministry of Land and Resources, China. The analytical uncertainties are ± 2% for major elements, ± 5% for rare-earth elements, and ± 5–10% for other trace elements. The regular settings of laser source, mass spectrometer, and standardization were described in detail by Liu et al. (2008). The results are listed in Table 4.

3.4. Sr and Nd isotopic compositions

Five samples were selected for whole-rock Rb–Sr and Sm–Nd isotopic analyses. Sr–Nd isotopic compositions were determined using a Micromass Isoprobe multi-collector ICP–MS at the State Key Laboratory of Isotope Geochemistry, the Guangzhou Institute of Geochemistry, Chinese Academy of Sciences, in accordance with the analytical procedures described by Li et al. (2004). Strontium and Nd were separated using cation columns, and Nd fractions were further separated by HDEHP-coated Kef columns. The measured $^{87}Sr/^{86}Sr$ ratio of the NBS 987 standard and $^{143}Nd/^{144}Nd$ ratio of the JNdi-1 standard were 0.710274 ± 18 (n =11, 2σ) and 0.512093 ± 11(n = 11, 2σ), respectively. All measured Nd and Sr isotope ratios were normalized to $^{146}Nd/^{144}Nd$ = 0.7219 and $^{86}Sr/^{88}Sr$ = 0.1194, respectively. The Sr–Nd isotope data are given in Table 5.

5. Results

5.1 U–Pb zircon dating

5.1.1 Mafic dikes

Sample S31 is from the mafic dike within the Sanligang pluton (Fig.1c). More than 100 zircon grains were separated from 45 kg rocks. Veins, alteration and weathering products were avoided during sample collection and preparation. The zircon grains are light pink to colorless and 30 to 90 μm in length. Most grains are euhedral to subeuhedral and have clear magmatic oscillatory zoning in cathodoluminescence (CL) images (Fig.4a). All analyses display Th/U ratios higher than 0.2 and mostly range from 0.47 to 0.87 (Table 2)

Seventeen spots were analyzed; and all analyses plot on or near the Concordia line and yield a weighted average $^{206}Pb/^{238}U$ age of 871 ± 7 Ma (MSWD = 1.3) (Fig. 4a). This age is interpreted to be the crystallization age that is younger than the Yangjiapeng MORB-type gabbro age of 947 ± 14 Ma (Fig. 1c, Shi et al., 2007).

5.1.2. Granitoids

Three granitoid samples (i.e., S04, S07, and S10) from the Sanligang pluton were used for zircon U-Pb dating. Sample S07 was dated by the SIMS method, whereas samples S04 and S10 were dated by LA–ICP–MS. U–Pb Concordia diagrams of the analyzed zircons are shown in Figs. 4b to 4d. The zircons are transparent to sub-translucent and 60–180 μm long. Most grains are subhedral to euhedral with well-developed pyramidal faces. These grains show oscillatory zoning (Figs. 4b to 4d) and have high Th/U ratios (0.46–0.87) (Table 2), indicating magmatic origins.

Eighteen points on 18 zircon grains from sample S07 plot on, or near the Concordia line (Fig. 4b). These grains have $^{206}Pb/^{238}U$ ages that range from 854 to 876 Ma with a weighted mean of 862 ± 5 Ma (MSWD = 0.33).

Fourteen zircon grains from sample S10 were analyzed and most analyses plot close to the Concordia line (Fig. 4c). Except for two analyses that deviated the Concordia line (spots S10-3 and S10-7), the remaining 12 analyses yield ages that range from 845 to 892 Ma with a weighted mean $^{206}Pb/^{238}U$ age of 866 ± 10 Ma (MSWD = 1.8).

Fifteen spots were analyzed on 15 zircons from sample S04 (Fig. 4d). Most of the data plot on or near the Concordia line. Six analyses show discordant $^{207}Pb/^{235}U$ and $^{206}Pb/^{238}U$ ages, whereas the other nine concordant analyses yield a weighted mean $^{206}Pb/^{238}U$ age of 858 ± 15 Ma (MSWD = 1.6).

5.2 Major and trace element compositions

5.2.1 Mafic dikes

Mafic dikes are characterized by high FeO (9.27–12.17 wt.%), MgO (6.25–9.85 wt.%), and CaO (8.83–10.57 wt.%), as well as low SiO_2 (45.37–49.73 wt.%), Al_2O_3 (13.29–16.13 wt.%), K_2O （0.32–1.13 wt.%） and Na_2O+K_2O (2.47–3.67 wt.%) (Table 4, Figs. 5 and 6). Thus, the mafic dikes belong to a low- to medium-K subalkaline series (Figs. 5d and 6g). Correspondingly, the rocks show sub-alkaline affinity in the Zr/TiO_2 vs. SiO_2 and Nb/Y vs. Zr/TiO_2 diagrams (no shown).

The trace element contents of all samples are low at ∑REE (45.4–87.2 ppm) (Table 4). All mafic dike samples show flat to slightly LREE-enriched chondrite-normalized patterns and insignificant Eu anomalies (Eu/Eu*=0.69–1.08) with low La/Yb_N (1.22–3.03) values (Fig. 7a). In the primitive mantle-normalized trace element variation diagrams, the samples are characterized by the selective enrichment of large ion lithophile elements (LILEs, such as Rb, Ba, Pb and Sr) and the depletion of high-field strength elements (HFSEs, such as Ta, Nb and Ti) (Fig. 7b).

5.2.2. Granitoids

Fourteen granitoid samples, including nine granodiorites and five quartz diorites, were analyzed for major and trace elements. These samples comprise SiO_2 (60.4–71.4 wt.%), Al_2O_3 (14.09–16.42 wt.%), K_2O (1.38–3.67 wt.%), and Na_2O (3.97–5.33 wt.%). Their total alkalis (K_2O+Na_2O) vary from 6.0 to 7.9 wt.% with low K_2O/Na_2O ratios (0.28–0.87). These rocks have relatively high TiO_2 (0.44–0.87 wt.%), TFeO(2.03–5.91 wt.%), P_2O_5(0.10%–0.18 wt.%), and MgO (1.03%–3.16 wt.%) (Fig. 6) with Mg# of 49 to 58. The samples fall into calcic–alkalic or alkalic–calcic field on the SiO_2 versus (K_2O+Na_2O–CaO) diagram (Fig. 5a), and plot in the I-type granitic rock field in the A/NK vs. A/CNK diagram (Fig. 5b), with A/CNK ratios between 0.84 and 1.04. They have low FeO/(FeO–MgO) ratios that are typical of the magnesian series (Frost et al., 2001; Fig. 5c). The TAS plot of rock classification diagram shows that the Sanligang samples fall into the diorite–monzonite–granodiorite field with only one sample plot in the granite field (Fig. 5d). Correspondingly, all samples plot in the rhyodacite/dacite field in the Nb/Y vs. Zr/TiO_2 diagram (no shown), which is consistent with the petrographic and TAS classification results.

The Sanligang granitoid samples have slightly variable REE contents (89.00–156.02 ppm), but similar chondrite-normalized REE patterns (Fig. 7c). All granitoid samples are enriched in LREEs with La/Yb_N = 7.14–12.3, and have slightly negative Eu anomalies (Eu/Eu* = 0.57–0.96) in the chondrite-normalized REE distribution diagrams. Their primitive mantle-normalized trace element patterns are characterized by enrichment of LILEs such as Rb, Ba, Th, U, and K, but depletion of Nb, Ta, P, and Ti with positive Pb and Hf anomalies compared with the neighboring elements (Fig.7d). They are also moderately enriched in V (46–145 ppm), Cr (19–98 ppm) and Ni (11–44 ppm).

5.3 Zircon Hf isotopic compositions

Lutetium–Hf isotopic analyses were conducted on the zircon grains of the same or similar structures that were previously analyzed for U–Pb isotopes. Initial $^{176}Hf/^{177}Hf$ ratios and $\varepsilon_{Hf}(t)$ values were calculated by using their U-Pb ages, registering the timing of zircon growth from magmas (Table 3).

Eighteen analyses were conducted on zircons from sample S31 collected from the Sanligang mafic dike. The $^{176}Lu/^{177}Hf$ and $^{176}Hf/^{177}Hf$ ratios of the zircons range from 0.000514 to 0.001713 and 0.282536 to 0.282614, respectively. Initial $^{176}Hf/^{177}Hf$ ratios range from 0.282525 to 0.282593, whereas the $\varepsilon_{Hf}(t)$ values range from +10.5 to +12.9 with an average of +11.4 ± 0.3. Their single-stage model ages (T_{DM1}, error 2σ) range from 910 to 1005 Ma with an average age of 971 ± 21 Ma (Figs. 8a and 8b).

Three samples (i.e., S07, S10, and S04) from the Sanligang pluton were collected for zircon analysis, and 48 spot analyses were analyzed. Their $^{176}Lu/^{177}Hf$ ratios range from 0.000388 to 0.001475, whereas their $^{176}Hf/^{177}Hf$ ratios range from 0.282470 to 0.282590. These results infer that the zircons from these three granitoid samples show similar $(^{176}Hf/^{177}Hf)_i$ values and positive $\varepsilon_{Hf}(t)$ values. In particular, the average $(^{176}Hf/^{177}Hf)_i$ values for the samples are 0.282518 (S07), 0.282495 (S10), and 0.282533 (S04). All analyses yielded positive $\varepsilon_{Hf}(t)$ values (+7.9 to +11.7) with an average of +10.1 (S07), +9.4 (S10) and +10.6 (S04). The average T_{DM1} of samples S07, S10, and S04 are 1014 ± 25 Ma, 1047 ± 31Ma, and 993 ± 24Ma, respectively (Figs. 8c, 8d and 9a). These features show that these zircons were crystallized from the same host magma.

5.4. Whole rock Sr–Nd isotopic compositions

The initial Sr–Nd isotopes were recalculated at 871 and 862 Ma for mafic dikes and granitoids, respectively. Two samples from the mafic dikes have relatively homogeneous initial $^{87}Sr/^{86}Sr$ ratios that range from 0.7051 to 0.7057 and positive $\varepsilon_{Nd}(t)$ values that range from +4.0 to +7.1 (Table 5 and Fig.9b). samples from the Sanligang granitoids have low and constant initial $^{87}Sr/^{86}Sr$ ratios ranging from 0.7033 to 0.7041 and uniform positive $\varepsilon_{Nd}(t)$ values (+3.4 to +4.9). On the $^{87}Sr/^{86}Sr$ versus $\varepsilon_{Nd}(t)$ diagram, the samples plot near the mantle array. The $\varepsilon_{Nd}(t)$ values of granitoid are near or slightly lower than the mafic values of the region (Fig. 9b). It is noteworthy that the Rb/Sr ratios of the mafic dikes are very low at 0.02-0.15 (Table 4). The mafic dikes show higher initial $^{87}Sr/^{86}Sr$ ratios (0.7051–

0.7057) than the granitoid (0.7033–0.7041), which may have been resulted from the alteration (Fig. 3a). Thus，the Sr isotopes for mafic dikes may be not reliable for these analyses.

6. Discussion

6.1. Petrogenesis of the mafic dikes

Samples from the Sanligang mafic dikes have low LOI (2.16–3.99 wt.%), indicating that they underwent minor low-temperature alteration. Aluminum, Ca, and Mg and HFSEs generally remain immobile during low-temperature alteration (Beswick, 1982; Barnes et al., 1985). The mafic dikes show narrow ranges of K_2O (0.32–0.95 wt.%), Na_2O (2.01–3.25 wt.%), Rb (5.02–20.4 ppm), and constant K_2O/Na_2O (0.11–0.38) as well as K_2O/Rb ratios (290–559). These features indicate that the alteration did not significantly modify their original chemical compositions. Accordingly, we will mainly focus on the HFSEs and Hf-Nd isotopic compositions to constrain their petrogenesis.

Crustal contamination can result in depletion of Nb and Ta but elevated Pb, Zr, and Hf concentrations (Zhao et al., 2010b). Although negative Nb anomalies and positive Pb anomalies are observed in the spider diagram (Fig. 7b), the relatively positive Ta anomalies contradict with strong crustal contamination. This conclusion is also supported by their Th (0.34–1.42 ppm), U (0.08–0.27 ppm), and Rb (5.02–20.4 ppm) that are lower than those of the upper crust (Th = 10.5 ppm, U = 2.7 ppm, Rb = 84 ppm; Rudnick and Gao, 2003). They also have uniform and positive ε_{Hf} (+10.5 to +12.9) and ε_{Nd} (+4.0 to +7.1) values (Figs. 8 and 9), arguing against involvement of significant crustal contamination in their petrogenesis.

The mafic dikes have higher Zr/Nb ratios (28.48–51.93) than those of OIB (5.83; Sun and McDonough, 1989), ruling out their derivation from the asthenospheric mantle. These samples have low Ta (0.24–0.64 ppm) and Nb concentrations (1.64–5.09 ppm). They also have low Nb/La (0.33-0.65) and Hf/Th (2.55-11.9), and high Hf/Ta (3.84-12.5), La/Ta (7.59-39.3), Th/Nb (0.15-0.41) and Th/Yb (0.10–0.46) ratios. These elemental contents and ratios are similar to those of arc basalts (Saunders et al., 1991; Pearce and Peate, 1995; Hawkins, 2003; Murphy, 2007). These samples exhibit flat to slight right-sloping chondrite-normalized REE patterns (Fig.7a), similar to those of the modern Barren Island island-arc basalts (IABs) in the Andaman Islands (Luhr and Haldar, 2006) (Fig.7b). In the primitive mantle-normalized trace element diagram (Fig.7b), they are characterized by large positive Rb, Ba, Pb and Sr anomalies, significantly negative Ta and Nb and weakly negative Ti anomalies, suggesting they were derived from a subduction modified mantle source. In the Nb-Zr-Y and Hf-Th-Nb diagrams (Figs. 10a and 10b), all samples plot in the island arc basalt field. Moreover, their relatively high Ba/Nb, La/Nb and low Nb/Th ratios suggest that they have an arc affinity geochemical compositions (Figs. 10c and 10d). On the plots of Nb/Yb vs. Th/Yb and Ta/Yb vs. Th/Yb (Figs. 10e and 10f), most samples plot in the field of oceanic arcs. Moreover, they have highly positive $\varepsilon_{Nd}(t)$ values and $\varepsilon_{Hf}(t)$ (Fig.9), suggesting that they were not derived from an ancient lithospheric source. Alternatively, the Sanligang mafic dikes were probably formed in an island arc setting.

Arc-related igneous rocks are generally considered to be originated from a mantle wedge that was modified by slab-derived fluids or melts (Münker, 2000; Murphy, 2007). The Sanligang mafic dikes have higher LILE/REE and LILE/HFSE ratios (i.e., Ba/Nb = 52–170, Ba/La = 18–97, Ba/Th = 161–1164, Pb/Nb = 0.46–3.50) than N-MORB and primitive mantle (Sun and McDonough, 1989), indicating that their source regions were modified by fluids derived from the subducted oceanic crust. This conclusion is supported by their H_2O-bearing minerals, such as amphiboles. Enrichment of slab-derived fluids could also explain the subchondritic Nb/Ta (4.1–17.0) and Nb/Th (2.4–6.9) ratios because such fluids would likely have low Nb/Ta and Nb/Th ratios due to the residual rutile in the slab (Münker, 1998). However, they have low Th (0.34–1.42 ppm), Nb (1.64–5.09 ppm) and Nd (9.31–17.2 ppm), and low Th/Y (0.01–0.05) and Th/Nb (0.15–0.41) ratios, suggesting that the mantle source was not modified by slab melts (Class et al., 2000). In summary, the arc-affinity geochemical characters of the Sanligang mafic dikes were inherited from the mantle source that was modified by slab-derived fluids in an arc setting.

6.2. Petrogenesis of the Sanligang granitoids

The Sanligang granitoids have low LOI (1.08–2.35 wt.%) (Table 4). These granitoids also have narrow variations of Na_2O (3.97–5.33 wt.%), Ba (396–763 ppm), and Rb (17–59 ppm), suggesting that they were not significantly modified by alteration. They show suitable correlations for K_2O and Sr against CaO, which indicates that K_2O and Sr were mainly controlled by Ca-bearing minerals (Figs. 6i and 6j), rather than alteration. Both their major and trace elements show linear correlations against SiO_2 (Figs.6a–6e, 6h, and 7d). Therefore, their elemental compositions can be used to interpret the origin of the Sanligang granitoids.

6.2.1. Classification of the Sanligang granitoids

Granitoids are usually divided into I-, S-, and A- type granites on the basis of their differences in petrography and geochemical composition (Barbarin, 1999, Chappell and White, 2001; Frost et al., 2001). Unlike S-type granites, I-type granites generally have high Na_2O and CaO, but low K_2O and alumina saturation (A/CNK) with more regular compositional variations (Chappell and White, 2001). The Sanligang granitoids display linear trends in major elemental diagrams (Fig. 6). They also have low K_2O/Na_2O ratios (0.28–0.87) and A/CNK values (0.84–1.04), suggesting that the Sanligang granitoids are I-type rather than S-type granites.

I- and S-type granites are mineralogically and geochemically different from A-type granites (Whalen et al., 1987). The Sanligang granitoids contain abundant amphibole (5–18%) and minor sphene and clinopyroxene (Table 1, Fig. 3). Although some differentiated samples have slightly higher K_2O values (Fig. 6g), the mineralogical and geochemical characteristics of the Sanligang granitoids indicate that they are similar to the amphibole-rich calc-alkaline granitoids in accordance with Barbarin's (1999) classification (Fig. 5). The Sanligang granitoids have low FeO/MgO (1.43–2.05), $(Na_2O+K_2O)/CaO$ (1.43–4.64), and 10000Ga/Al (1.87–2.78) ratios. They also have low concentrations of HFSEs and REEs. For example, their Nb contents range from 5.03 ppm to 9.24 ppm, Zr from 94 ppm to 259 ppm, and Zr+Nb+Ce+Y from 148 ppm to 320 ppm. These chemical compositions are significantly different from those of A-type granites but similar to those of I-type granites. Although the Sanligang granitoids have a wide range of silica contents (SiO_2=60.35–71.38 wt.%), they show uniform initial $^{87}Sr/^{86}Sr$ ratios (0.7033–0.7041), positive ε_{Nd} (t) (+3.4 to +4.9), and ε_{Hf}(t) values (+7.9 to +11.7) (Fig. 9). All these features imply that the Sanligang granitoids are I-type rather than A-type.

Moreover, the Sanligang granitoids are characterized by enrichments in LREEs and LILEs but depletions in HREEs and HFSEs (Figs. 7d) with some characteristics of arc magma originating from the subduction zone environment (Sun and McDonough, 1989; Murphy, 2007). All granitoid samples plot in the field of the volcanic arc granite in the tectonic discrimination diagrams (Figs. 10g and 10h). Thus, the rocks from the Sanligang granitoid are interpreted as I-type granites with distinguished magmatic arc signatures.

6.2.2 Petrogenesis of the Sanligang granitoids

I-type granites can be generated by the differentiation of basaltic magmas (White and Chappell, 1977; Zhao et al., 2013b), mixing of basaltic magma with felsic magmas, interaction of basaltic magmas with continental crust (Chappell, 1996; Janousek et al., 2004), and melting of basaltic crust (Chappell and White 2001).

Granites generated by the mixing of mafic magma with crustal-derived felsic magma are characterized by abundant mafic enclaves and a wide range of chemical compositions (Chappell 1996; Janousek et al., 2004; Wang et al., 2012). The Sanligang granitoids have SiO_2 contents that are much higher than those of the mafic dikes (Fig. 6), suggesting that voluminous crustal materials would have been required. However, they have a narrow range of initial $^{87}Sr/^{86}Sr$ (0.7033–0.7041), $\varepsilon_{Nd}(t)$ (+3.4 to +4.9) and $\varepsilon_{Hf}(t)$ (+7.9 to +11.7). Their $\varepsilon_{Hf}(t)$ values are similar to those of the mafic rocks in the region (Fig. 9), suggesting that minor old crustal materials were involved in their petrogenesis.

6.2.2.1 Differentiation of mantle-derived magmas

I-type granites are generally produced by the differentiation of mantle-derived magmas (White and Chappell, 1977). This type of granitoid is characterized by high Mg#, Ni, and Cr (Smithies and Champion, 2000). For example, the ca. 850 Ma Huangling tonalites show similar elemental and isotopic compositions to those of the Huangling mafic dikes, and are thought to have been produced by differentiation of the mantle-derived melts (Zhao et al., 2013b) (Figs. 9). The Neoproterozoic mafic rocks are widely distributed in the SSFB (Dong et al., 2004). The mafic dikes and granitoids in this study have similar zircon U-Pb ages and Hf isotopic compositions (Fig. 9), suggesting that they were probably derived from the same source region. These mafic dikes are the only mantle-derived rocks that can possibly represent the protolith of the Sanligang granitoids. However, significant compositional gaps exist between the Sanligang granitoids and the mafic rocks (Figs. 6-7), suggesting the Sanligang granitoids were not differentiation products of the mantle-derived magmas.

Unlike the mantle-derived high-Mg granitoids (Stern and Hanson, 1991; Smithies and Champion, 2000), the Sanligang granitoids have lower MgO (1.03–3.51 wt.%), Ni (11–44 ppm), and Cr (mostly less than 70 ppm) contents, and low Mg# values (49–58). They also have relatively high La (15.8–28.4 ppm), Sm (3.6–6.0 ppm), and Th (1.8–10.7 ppm) and low Sc (4.5–17.6 ppm), which cannot be achieved by high degrees of fractional crystallization from mafic magmas. For example, the removal of 80% mafic minerals from the proposed parental magma, represented by the average composition of the mafic intrusions, increases Th from its initial concentration to 3.0 ppm (Zhao and Zhou, 2009b). But the Th concentrations of the Sanligang granitoids are mostly higher than 3.0 ppm, which contradicts the derivation by the differentiation of mantle-derived magmas. Therefore, the possibility of differentiation of basaltic magmas should be ruled out.

6.2.2.2 Parting melting of basaltic crust

I-type granites can be formed by melting of basaltic crust (Chappell and White 2001, Zhao and Zhou, 2008, 2009a; Zhao et al., 2010a, 2013a). The ancient basement of the Yangtze Block is mainly composed of Archean and Paleoproterozoic rocks (Gao et al., 1999). The Neoproterozoic granitoids (e.g., Huangling trondhjemites and TTG-like rocks) (Fig. 9) from the Central Yangtze Block produced by the melting of these ancient continent crustal rocks generally show extremely negative ε_{Nd} (< -19) and zircon Hf values (< -19) (Zhao et al., 2013b; Zhang et al., 2009). However, the Sanligang granitoids have low initial $^{87}Sr/^{86}Sr$ (0.7033–0.7041) and positive ε_{Nd} (t) (+3.4 to +4.9) and zircon ε_{Hf} (t) values (+7.9 to +11.7) (Fig. 9), suggesting that they were probably formed by the partial melting of juvenile crust, rather than derived from ancient continental crust rocks.

The Sanligang granitoids could have been produced by partial melting of subducted oceanic slab that have MORB-like Nd isotopic compositions (e.g., Sajona et al., 2000). The slab-derived melts have adakitic compositions that have high Sr/Y and La/Yb ratios with positive Eu anomalies (Defant and Drummond, 1990). However, the Sanligang granitoids do not have such positive Eu anomalies. They have low to moderate Sr (243–551 ppm) and high Y (12.4–18.9 ppm) and Yb (1.3–1.8 ppm) concentrations, which yield low Sr/Y (14–43) and La/Yb (10–17) ratios. Most Sanligang samples plot in the normal arc magma field in the plots of Sr/Y vs. Y and Yb_N vs. $(La/Yb)_N$ (Figs. 11a and 11b). Thus, they are chemically different from the oceanic slab-derived adakites.

Alternatively, the Sanligang granitoids could have been generated by the melting of newly formed mafic continental crust. The partial melting of newly formed lower mafic crust can produce silicic magmas with initial isotopic values the similar to their mafic sources (e.g., Hannan adakitic rocks, Tianpinghe granits, Xixiang diorites and Huangling granites, Fig. 9) (Zhao and Zhou, 2008, 2009a; Zhao et al., 2010a, 2013a). The occurrence of mafic rocks in the SSLB implies that the Neoproterozoic period was crucial for continental crust growth. The granitoids have narrow ranges of positive $\varepsilon_{Nd}(t)$ (+3.4 to +4.9) and $\varepsilon_{Hf}(t)$ values (+7.9 to +11.7) that are similar to those of the mafic dikes ($\varepsilon_{Hf}(t)$ = +10.5 to +12.9, $\varepsilon_{Nd}(t)$ = +4.0–+7.1), respectively. These features indicate that both granitoids and mafic dikes originated from similar sources (Fig. 9). Moreover, the granitoids and mafic dikes form a coherent trend in the plot of Th/Tb vs. Th/Ta (Fig. 11c). This result further supports the conclusion that the source region of the granitoids is chemically similar to that of the mafic dikes.

Experimental results show that silicic to intermediate calc-alkaline magmas are normally generated by the dehydration melting of fertile portions of the continental crust at high temperatures (Rapp and Watson, 1995). All samples in this study plot in the field of the experimental melts in the plot of TiO_2 vs. SiO_2 that were produced at high temperature (1000–1100 °C) but relatively low pressures (Fig. 6e; Rapp and Watson, 1995). However, the samples plot in or near the field of the experimental melts in the plot of MgO vs. SiO_2 (Fig. 6b). In the SiO_2 vs. Mg# diagram (Fig. 11d), the Sanligang granitoids are approximately similar to hybridized melts and sanukitoids, suggesting that additional mafic materials were involved in their source region. The partial melting of subducted oceanic slab or delaminated continental lower crust and the possible following interaction with mantle peridotite can be considered to explain the origin of the high-Mg diorites (e.g., Martin, 1999; Gao et al., 2004). However, melts that were derived from the subducted oceanic slab or delaminated lower crust typically display an adakitic affinity, which contrast with the relatively low Sr/Y and $(La/Yb)_N$ ratios in the Sanligang granitoids (Figs. 11a and 11b). Interaction between the intermediate magmas and the mafic residue is an important process in the formation of the Mg-rich dioritic igneous rocks (Zhao et al., 2010a). The high Mg# values of the Sanligang granitoids were probably resulted from interaction between crust-derived felsic melts and mafic residues. This model can also account for their relatively high CaO, FeO, Cr and Ni contents The Sanligang granitoids are therefore interpreted to have been generated by melting of the newly formed mafic crust followed by interaction with the mafic residues.

6.3. Implications for records of the early Neoproterozoic subduction of oceanic slab

Previous studies proposed that the SSFB is part of the Phanerozoic suture zone between the Yangtze Block and the Tongbai orogen (Dong et al., 1999, 2004; Lai et al., 2004). Our new age data obtained from the SSFB provide a new perspective on these oceanic crust-related rocks. Given the MORB-type gabbros (Figs. 10a-e, Shi et al., 2005; 2007) (Fig. 1c), the oceanic subduction in the northern margin of the Yangtze Block could have started no later than 947 Ma. The 871 Ma mafic dikes in this study show arc-like geochemical compositions that were produced by the partial melting of a subduction-modified mantle wedge. The 860 Ma Sanligang I-type granitoids also show arc signatures. Their geochemical and Hf-Nd isotopic compositions reveal that the granitoids were produced by melting the newly formed mafic crust above the oceanic subduction zone.

A magmatic arc sequence exposed in the Shennongjia dome (1.15–0.90 Ga, Qiu et al., 2011) and the Miaowan "ophiolite" (1.10–0.98 Ga, Peng et al., 2012)) has been recently reported in the west of the SSFB (Fig. 12). Considering the very close temporal and spatial relationships, we propose that the Miaowan-Shennongjia accretionary wedge-arc system formed to the east of the Sanligang pluton. The early Neoproterozoic igneous rocks from SSFB represent an oceanic subduction zone in the northern margin of the Yangtze Block (Fig. 12).

Whether or not 850–750 Ma arc-affinity rocks are formed by arc magmatism or by melting of pre-existing juvenile arc rocks in an anorogenic setting has been a hotly-debated issue (Li et al., 2003a; 2003b; Wang et al., 2009; Huang et al.; 2009). The arc-affinity granitoids and mafic igneous rocks in the present study indicate that the oceanic subduction occurred at approximately 860 Ma. The arc setting is also supported by the 1.1–0.9 Ga Miaowan ophiolite–Shennongjia arc association that was found in the west of the SSFB (Fig.12). This arc-continent collision did not happen until ca. 870–850 Ma (Peng et al., 2012). A number of 880–800 Ma arc-related calc-alkaline dioritic rocks (Xiao et al., 2007; Sun and Zhou, 2008; Wang et al., 2012; Zhao et al., 2013b; Du et al., 2014), especially arc-related mafic extrusive-intrusive rocks (Zhou et al., 2002, 2006; Lai et al., 2007; Dong et al., 2012; Zhao and Zhou, 2007, 2009b, 2010b; Wang et al., 2008;), were reported at the regional scale. Such reports provide strong evidence for an arc setting at approximately 860 Ma. In addition, the time span of nearly 90 Ma between 974 Ma (Yangjiapeng gabbro) and 858 Ma (Sanligang granitoid) is inconsistent with an anorogenic setting such as the plume-rift model (e.g., Li et al., 2003a).

Previous studies have identified many subduction–accretion–arc formations in the periphery of the Yangtze Block (Zhang et al., 2013a). The 1.0–0.8 Ga Panxi–Hannan arc rocks are distributed along the northwestern margin of the Yangtze Block, from Kanding–Danba in the west to Bikou–Hannan–Micangshan and Mian–Lue in the northwest (Bader et al., 2013; Zhao and Cawood, 2012). Many arc-related rocks or blocks from the Panxi–Hannan belt indicate the presence of a Neoproterozoic oceanic basin outboard (northwest in present coordinates) of the Yangtze Blocks. The ocean was subducted southward beneath the Yangtze Block, which led to the eruption of many arc-related volcanic rocks now assigned to the Yanbian Group (> 860 Ma, Sun et al., 2008), Xixiang Group (950–890 Ma, Ling et al., 2003), and Bikou Group (880–770 Ma, Wang et al., 2008). The oceanic subductution also led to the emplacement of calc-alkaline intrusive rocks (i.e., adakite, diorite, tonalite, and granodiorite) (Xiao et al., 2007; Zhao and Zhou, 2007; Sun and Zhou, 2008; Zhao et al., 2013b; Du et al., 2014). The subduction model provides the simplest approach to explain the tectonic setting of early Neoproterozoic igneous rocks in the northwestern margin of the Yangtze Block. Some calc–alkaline granitoids from the Panxi–Hannan arc have extremely positive $\varepsilon_{Hf}(t)$ and $\varepsilon_{Nd}(t)$ values, with the highest value approximating those of the contemporaneous depleted mantle (Sun and Zhou, 2008; Du et al., 2014), suggesting the growth of juvenile crust. Some high-K granitoids from the Huangling region show extremely negative $\varepsilon_{Hf}(t)$ and $\varepsilon_{Nd}(t)$ values, and the Archean Hf-Nd model ages for them, which represents the partial melting of ancient continental crust rocks (Zhang et al., 2009; Zhao et al., 2013b). Both mafic dikes and granitoids from the SSFB have high positive $\varepsilon_{Hf}(t)$ and $\varepsilon_{Nd}(t)$ values, which indicate juvenile crust growth and crustal reworking. Similar examples have been widely reported for the Hannan and Huangling regions (Figs. 9 and 12). Thus, the early Neoproterozoic is an important period of continental crust growth and reworking, and the oceanic crust subduction has played a central role in these processes.

7. Conclusion

(1) The Sanligang mafic dikes (871 Ma) have arc-like geochemical features characterized by enrichment of LILEs and depletion of HFSEs. New elemental and isotopic data suggest that these mafic dikes were derived from the depleted mantle source enriched by slab-derived fluids above a subducting oceanic slab and were emplaced in an island arc environment.

(2) The Sanligang pluton (860 Ma) is dioritic to granitic in composition and has positive and high $\varepsilon_{Hf}(t)$ and $\varepsilon_{Nd}(t)$ values similar to those of the mafic dikes. It was produced by high degree melting of the juvenile basaltic crust followed by interaction with the mafic residues. Based on its arc-related geochemical affinity and contemporaneous arc-related magmatism, the Sanligang pluton is proposed to have been generated in a Neoproterozoic arc setting during continental crustal growth and reworking of the Yangtze Block.

(3) The early Neoproterozoic igneous assemblage from the Sangligang-Sanyang fault belt provides an important record of oceanic-slab subduction in the northern margin of the Yangtze Block.

Acknowledgment

We sincerely thank Prof. Jun-Hong Zhao for his constructive suggestions that have improved the manuscript. We are grateful to the official reviews by two anonymous reviewers and editorial handling by Editor Prof. Guo-Chun Zhao. This paper was financially supported by the National Natural Sciences Foundation of China (Grants Nos. 41172189, 40972137 & 41402179).

Reference

Andersen, T., 2002. Correction of common lead in U-Pb analyses that do not report ^{204}Pb. *Chemical Geology* 192, 59-79.

Bader, T., Ratschbacher, L., Franz, L., Yang, Z., Hofmann, M., Linnemann. U., Yuan. H. L., 2013. The heart of China revisited, I. Proterozoic tectonics of the Qin mountains in the core of supercontinent Rodinia. *Tectonics* 32, 661-687.

Barbarin, B., 1999. A review of the relationships between granitoid types, their origins and their geodynamic environments. *Lithos* 46, 605-626.

Barnes, S. J., Naldrett, A.J., Gorton, M.P., 1985. The origin of the fractionation of platinum-group elements in terrestrial magmas. *Chemical Geology* 53, 303-323.

Belousova, E., Suzanne, G.W., Fisher, Y., 2012. Igneous zircon: Trace ele-ment composition as an indicator of source rock type. *Contrib Mineral Petrol* 143, 602-622.

Beswick, A.E., 1982. Some geochemical aspects of alteration and genetic relations in komatiitic suites. In: Arndt, N.T., Nisbet, E.G. (Eds.), Komatiities. *George Allen & Unwin, London*, 283-308.

Blichert-Toft, J., Albarede, F., 1997. The Lu-Hf geochemistry of chondrites and the evolution of the mantle-crust system. *Earth and Planetary Science Letters* 148, 243-258.

Cawood, P.A., Wang, Y.J., Xu, Y.J., Zhao, G.C., 2013. Locating South China in Rodinia and Gondwana: a fragment of Greater Indian Lithosphere? *Geology*, http://dx.doi.org/10.1130/G34395.1.

Chappell, B. W., 1996. Magma mixing and the production of compositional variation within granite suites: evidence from the granites of southeastern Australia. *Journal of Petrology* 37(3), 449-470.

Chappell, B. W., White, A. J. R., 2001. Two contrasting granite types: 25 years later. *Australian Journal of Earth Science* 48, 489-499.

Charvet, J., 2013. The Neoproterozoic-Early Paleozoic tectonic evolution of the South China Block: An overview. *Journal of Asian Earth Sciences* 7, 198-209.

Chen, W.T., Sun, W.H., Zhao, J.H., Wang, W., Zhou, M.F., 2014. "Grenvillian" intra-plate mafic magmatism in the southwestern Yangtze Block, SW China. *Precambrian Research* 242, 138-153.

Class, C., Miller, D. M., Goldstein, S. L., Langmuir, C. H., 2000. Distinguishing melt and fluid subduction components in Umnak Volcanics, Aleutian Arc. *Geochemistry, Geophysics, Geosystems* 1. doi:10.1029/1999GC000010.

Defant, M.J., Drummond, M. S., 1990. Derivation of some modern arc magmas by melting of young subducted lithosphere. *Nature* 347, 662-665.

Dilek,Y., Furnes, H., 2011. Ophiolite genesis and global tectonics: geochemical and tectonic fingerprinting of ancient oceanic lithosphere. *Geological Society of America Bulletin* 123, 387-411.

Dong, S.W., Hu, J. M., Li, S. Z., Shi, W., Gao, R., Liu, X. C., Xue, H.M., 2005. The Jurassic deformation in the Dabie Mountains and its tectonic significances. *Acta Petrologica Sinica* 21(4):1189-1194.

Dong, Y. P., Liu, X. M., Santosh, M., Chen, Q., Zhang, X. N., Li, W., He, D. F., Zhang, G. W., 2012. Neoproterozoic accretionary tectonics along the northwestern margin of the Yangtze Block, China: Constraints from zircon U-Pb geochronology and geochemistry. *Precambrian Research* 196-197, 247- 274.

Dong,Y. P., Zhang, G. W., Lai, S. C., Zhou, D. W.，Zhu, B. Q., 1999. An ophiolitic tectonic melange first discovered in Huashan area, south margin of Qinling Orogenic Belt, and its tectonic implications. *Science in China: Earth Sciences* 42(3)，292-302.

Dong, Y. P., Zhang, G. W., Yao, A. P., Zhao, X., 2003. Deformation and evolution of the Sanligang- Sanyang tectonic melange belt along the west sector of Xiangfan-Guangji fault. *Chinese journalof geology* 28(4):425-436.

Dong, Y P, Zhang G W, Zhao X, Yao A P, Liu X M. 2004. Geochemistry of the subduction-related magmatic rocks in the Dahong Mountains, northern Hubei Province——Constraint on the existence and subduction of the eastern Mianlüe oceanic basin. *Science in China: Earth Sciences* 47(4)，366-377.

Du, L. L., Guo, J. H., Nutman, A. P., Wymand, D., Geng, Y. S., Yang, C. H., Liu, F. L., Ren, L. D., Zhou, X.W., 2014. Implications for Rodinia reconstructions for the initiation of Neoproterozoic subduction at –860 Ma on the western margin of the Yangtze Block: Evidence from the Guandaoshan Pluton. *Lithos* 196-197, 67-82.

Elliott, T., Plank, T., Zindler, A., White, W., Bourdon, B., 1997. Element transport from slab to 678 volcanic front at the Mariana Arc. *Journal of Geophysical Research* 102 (14), 991–1015, 019.

Fan, W.M., Guo, F., Wang, Y.J., Zhang, M., 2004. Late Mesozoic volcanism in the northern Huaiyang tectono-magmatic belt, central China: partial melts from a lithospheric mantle with subducted continental crust relicts beneath the Dabie orogen? *Chemical Geology* 209, 27–48.

Frost, B. R., Barnes, C. G., Collins, W. J., Arculus, R. J., Ellis, D. J., Frost, C. D., 2001, A geochemical classification for granitic rocks. *Journal of Petrology* 42(11), 2033-2048.

Gao, S., Ling, W.L., Qiu, Y.M., Lian, Z., Hartmann, G., Simon, K., 1999. Contrasting geochemical and Sm-Nd isotopic compositions of Archean metasediments from the Kongling high-grade terrain of the Yangtze craton: evidence for cratonic evolution and redistribution of REE during crustal anatexis. *Geochimica et Cosmochimica Acta* 63, 2071-2088.

Gao, S., Rudnick, R.L., Yuan, H. L., Liu, X. M., Liu, Y. S., Xu, W. L., Ling, W. L., Ayers, J., Wang, X. C., Wang, Q. H., 2004. Recycling lower continental crust in the North China craton. *Nature* 432, 892-897.

Geng, Y. S., Yang, C.H., Wang, X. S., Du, L. L., Ren, L.D., Zhou, X. W., 2008. Metamorphic Basement Evolution in Western Margin of Yangtze Block. *Geological Publishing House, Beijing,* 1-215 (in Chinese).

Griffin, W.L., Pearson, N.J., Belousova, E.A., Saeed, A., 2006. Comment: Hf-isotope heterogeneity in zircon 91500. *Chemical Geology* 233, 358-363.

Hawkins, J.W., 2003. Geology of supra-subduction zones-Implications for the origin of ophiolites. In: Dilek, Y., Newcomb, S. (Eds.), Ophiolite Concept and the Evolution of Geological Thought. Geological Society of America Special Paper 373, 227-268.

HBBGMR (Hubei Bureau of Geology and Mineral Resources), 1982. 1:200 000 geological map of Suixian.

Huang, X. L., Xu. Y. G., Lan, J. B., Yang, Q. J., Luo, Z. Y., 2009. Neoproterozoic adakitic rocks from Mopanshan in the western Yangtze Craton: Partial melts of a thickened lower crust. *Lithos* 112,367-381.

Hu, Z. C., Liu, Y. S., Gao, S., Liu, W. G., Zhang, W., Tong, X. R., Lin, L., Zong, K. Q., Li, M., Chen, H. H., Zhou, L., Yang, L., 2012. Improved in situ Hf isotope ratio analysis of zircon using newly designed X skimmer cone and jet sample cone in combination with the addition of nitrogen by laser ablation multiple collector ICP-MS. *Journal of Analytical Atomic Spectrometry* 27(9), 1391-1399.

Janousek, V., Braithwaite, C. J. R., Bowes, D. R., Gerdes, A., 2004. Magma-mixing in the genesis of Hercynian calc-alkaline granitoids: an integrated petrographic and geochemical study of the Sazava intrusion, Central Bohemian Pluton, Czech Republic. *Lithos* 78, 67-99.

Jung, S., Hoernes, S., Mezger, K., 2002. Synorogenic melting of mafic lower crust: constraints from geochronology, petrology and Sr, Nd, Pb and O isotope geochemistry of quartz diorites (Damara orogen, Namibia). *Contributions to Mineralogy and Petrology* 143, 551-566.

Lai, S. C., Li Y. F., Qin J. F., 2007. Geochemistry and LA-ICP-MS zircon U-Pb dating of the Dongjiahe ophiolite complex from the western Bikou terrane. *Science in China Series D: Earth Sciences* 50(Supp.), 305-313.

Lai, S. C., Zhang, G. W., Dong, Y. P., Pei, X.Z., Chen, L., 2004. Geochemistry and regional distribution of ophiolites and associated volcanics in Mianlüe suture, Qinling-Dabie Mountains. *Science in China Series D: Earth Science* 47(4), 289-299.

Ling, W. L., Gao, S., Zhang, B. R., Li, H. M., Liu, Y., Cheng, J. P., 2003. Neoproterozoic tectonic evolution of the northwestern Yangtze craton, South China: implications for amalgamation and break-up of the Rodinia Supercontinent. *Precambrian Research* 122, 11-140.

Ling, W.L., Ren, B.F., Duan, R. C., Liu, X. M., Mao, X. W., Peng, L. H., Liu, Z. X., Cheng, J. P., Yang, H. M., 2008. Timing of the Wudangshan, Yaolinghe volcanic sequences and mafic sills in South Qinling: U-Pb zircon geochronology and tectonic implication. *Chinese Science Bulletin* 53, 2192-2199.

Liu, Y. S., Hu, Z. C., Gao, S., Gunther, D., Xu, J., Gao, C. G., Chen, H. H., 2008. In situ analysis of major and trace elements of anhydrous minerals by LA-ICP-MS without applying at internal standard. *Chemical Geology* 257(1): 34-43.

Liu, Y. S., Gao, S., Hu, Z. C., Gao, C. G., Zong, K. Q., Wang, D.B., 2010. Continental and oceanic crust recycling-induced melt-peridotite interactions in the trans-north China Orogen: U-Pb dating, Hf isotopes and trace elements in Zircons from Mantle Xenoliths. *Journal of Petrology* 51(1-2): 537-571.

Li, X. H., Liu, D. Y., Sun, M., Li, W. X., Liang, X. R., Liu, Y., 2004. Precise Sm-Nd and U-Pb isotopic dating of the supergiant Shizhuyuan polymetallic deposit and its host granite, SE China. *Geological Magazine* 141, 225-231.

Li, X. H., Liu, Y., Li, Q. L., Guo, C. H., Chamberlain, K. R., 2009. Precise determination of Phanerozoic zircon Pb/Pb age by multicollector SIMS without external standardization, *Geochemistry Geophysics Geosystems* 10, Q04010, doi: 10.1029/2009GC002400.

Li, X. H., Li, Z. X., Ge, W. C., Zhou, H. W., Li, W. X., Liu, Y., Wingate, M. T. D., 2003a. Neoproterozoic granitoids in South China: crustal melting above a mantle plume at ca. 825 Ma?. *Precambrian Research* 122, 45-83.

Li, X. H, Li, Z. X, Zhou, H. W., Liu, Y., Kinny, P. D., 2002. U-Pb zircon geochronology, geochemistry and Nd isotopic study of Neoproterozoic bimodal volcanic rocks in the Kangdian Rift of South China: implications for the initial rifting of Rodinia. *Precambrian Research* 113, 135-154.

Li, X. H., Li, Z. X., Zhou, H. W., Liu, Y., Liang, X. R., Li, W. X., 2003b. SHRIMP U-Pb zircon age, geochemistry and Nd isotope of the Guandaoshan pluton in SW Sichuan: Petrogenesis and tectonic significance. *Science in China Series D: Earth Science* 46(Supp.), 73-83.

Li, Z. X., Bogdanova, S. V., Collins, A. S., Davidson, A., Waele, B. De., Ernst, R. E., Fitzsimons, I. C. W., Fuck, R. A., Gladkochub, D. P., Jacobs, J., Karlstrom, K. E., Lu, S., Natapov, L. M., Pease, V., Pisarevsky, S. A., Thrane, K., Vernikovsky, V., 2008. Assembly, configuration, and break-up history of Rodinia: A synthesis. *Precambrian Research* 160, 179-210.

Li, Z. X., Li, X. H., Kinny, P. D., Wang, J., Zhang, S., Zhou, H., 2003c. Geochronology of Neoproterozoic syn-rift magmatism in the Yangtze Craton, South China and correlations with other continents: evidence for a mantle superplume that broke up Rodinia. *Precambrian Research* 122, 85-109.

Li, Z.X., Zhang, L.H., Powell,C. M., 1995. South China in Rodinia: Part of the missing link between Australia-East Antarctica and Laurentia?. *Geology* 23, 407-410.

Ludwig, K.R., 2003. Users Manual for Isoplot 3.00: A Geochronological Toolkit for Microsoft Excel. *Berkeley Geochronology Center*, *Special*, Publication, 4.

Luhr, J.F., Haldar, D., 2006. Barren Island Volcano (NE Indian Ocean): Island-arc highalumina basalts produced by troctolite contamination. *Journal of Volcanology and Geothermal Research* 149, 177–212.

Martin, H., 1999. Adakitic magmas: modern analogues of Archaean granitoids. *Lithos* 46, 411-429.

Meschede, M., 1986. A method of discriminating between different types of midocean ridge basalts and continental tholeiites with the Nb–Zr–Y diagrams. *Chemical Geology* 56, 207–218.

Münker, C., 1998. Nb/Ta fractionation in a Cambrian arcrback arc system, New Zealand: source constraints and application of refined ICPMS techniques. *Chemical Geology* 144, 23–45.

Münker, C., 2000. The isotope and trace element budget of the Cambrian Devil River Arc System, New Zealand: identification of four source components. *Journal of Petrology* 41, 759-788.

Murphy, J.B., 2007. Arc magmatism II: geochemical and isotopic characteristics. Geoscience Canada 34, 7-35.

Pearce, J.A., 1983. Role of the sub-continental lithosphere in magma genesis at active continental margin. In: Hawkesworth, C.J., Norry, M.J. (Eds.), Continental Basalts and Mantle Xenoliths. *Shiva Publishing Ltd., Nantwich, Cheshire*, 230–249.

Pearce, J.A., Harris, N.W., Tindle, A.G., 1984. Trace element discrimination diagrams for the tectonic interpretation of granitic rocks. *Journal of Petrology* 25, 956-983.

Pearce, J.A., Peate, D.W., 1995. Tectonic implications of the composition of volcanic arc magmas. Annual Reviews of Earth and Planetary Sciences 23, 251-285.

Peng, S.B., Kusky, T. M., Jiang, X. F., Wang, L., Wang, J. P., Deng, H., 2012.Geology, geochemistry, and geochronology of the Miaowan ophiolite, Yangtze craton: Implications for South China's amalgamation history with the Rodinian supercontinent. *Gondwana Research* 21, 577-594.

Qiu, X. F., Ling, W. L., Liu, X. M., Kusky, T., Berkana, W., Zhang, Y. H., Gao, Y. J., Lu, S. S., Kuang, H., Liu, C. X., 2011. Recognition of Grenvillian volcanic suite in the Shennongjia region and its tectonic significance for the South China Craton. *Precambrian Research* 191, 109-119.

Rapp, R. P., Watson, E. B., 1995. Dehydration melting of metabasalt at 8-32 kbar: implications for continental growth and crust-mantle recycling. *Journal of Petrology* 36, 891-931.

Rudnick, P.L., Gao, S., 2003. 3.01 - Composition of the Continental Crust. *Treatise on Geochemistry* 3,1-64.

Sajona, F.G., Maury, R.C., Pubellier, M., Leterrier, J., Bellon, H., Cotten, J., 2000. Magmatic source enrichment by slab-derived melts in a young post-collision setting, central Mindanao (Philippines). *Lithos* 54, 173-206.

Saunders, A.D., Norry, M.J., Tarney, J., 1991. Fluid influence on the trace element compositions of subduction zone magmas. Philosophical Transactions of Royal Society London A., 335, 377-392.

Shi, Y. R., Zhang, Z. Q., Liu, D. Y., Tang, S. H., Wang, J. H., 2003. A Study on Sm-Nd, Rb-Sr Isotopic Chronology of the Huashan Ophiolitic Mélange in the Suizhou Area, Hubei Province. *Geological. Review* 49(4): 367-373 (in Chinese with English abstract).

Shi, Y. R., Zhang, Z. Q., Liu, D. Y., Tang, S. H., Wang, J. H., Liu, T. 2005. Rb-Sr Isotope Dating of Gabbro from Yangjiapeng Area in Suizhou, Hubei Province. *Acta Geoscientica Sinica (Chinese edition)* 26(6): 521-524 (in Chinese with English abstract).

Shi, Y. R., Liu, D. Y., Zhang, Z. Q., Miao, L. C., Zhang, F. Q., Xue, H. M., 2007. SHRIMP Zircon U-Pb Dating of Gabbro and Granite from the Huashan Ophiolite, Qinling Orogenic Belt, China: Neoproterozoic Suture on the Northern Margin of the Yangtze Craton. *Acta Geologica Sinica* 81(2), 239-243.

Sláma, J., Košler, J., Condon, D. J., Crowley, J. L., Gerdes, A., Hanchar, J. M., Horstwood, M. S. A., Morris, G. A., Nasdala, L., Norberg, N., Schaltegger, U., Schoene, B., Tubrett, M. N., Whitehouse, M. J., 2008. Plešovice zircon - A new natural reference material for U-Pb and Hf isotopic microanalysis. *Chemical Geology* 249, 1-35.

Smithies, R.H., Champion, D.C., 2000. The Archaean high-Mg diorite suite: links to tonalite-trondhjemite-granodiorite magmatism and implications for early Archaean crustal growth. *Journal of Petrology* 41, 1653-1671.

Stern, R. A., Hanson, G. N., 1991. Archean high-Mg granodiorite——a derivative of light rare-earth element-enriched monzodiorite of mantle origin. *Journal of Petrology*, 32, 201-238.

Sun, S. S., McDonough, W. F., 1989. Chemical and isotopic systematics of oceanic basalts: implications for mantle composition and processed. Magmatism in Ocean Basins. *Geological Society of London Special Publication* 42, 313-345.

Sun, W. H., Zhou, M. F., 2008. The–860Ma, Cordilleran-Type Guandaoshan Dioritic Pluton in the Yangtze Block, SW China: Implications for the Origin of Neoproterozoic Magmatism. magmatism. *The Journal of Geology* 116, 238-253.

Sun, W.H., Zhou, M.F., Yan, D.P., Li, J.W., Ma, Y.X., 2008. Provenance and tectonic setting of the Neoproterozoic Yanbian Group, western Yangtze Block (SW China). *Precambrian Research* 167, 213-236.

Wang, W., Liu, S. W., Feng, Y. G., Li, Q. G., Wu, F. H., Wang Z Q, Wang, R. T., Yang, P. G., 2012. Chronology, petrogenesis and tectonic setting of the Neoproterozoic Tongchang dioritic pluton at the northwestern margin of the Yangtze Block: Constraints from geochemistry and zircon U-Pb-Hf isotopic systematics. *Gondwana Research* 22, 699-716.

Wang, W., Zhou, M. F., 2012. Sedimentary records of the Yangtze Block (South China) and their correlation with equivalent Neoproterozoic sequences on adjacent continents. *Sedimentary Geology* 265-266, 126-142.

Wang, X. C., Li, X. H., Li, W. X., Li, Z. X., 2009. Variable involvements of mantle plumes in the genesis of mid-Neoproterozoic basaltic rocks in South China: A review. *Gondwana Research* 15, 381-395.

Wang, X.C., Li, X.H., Li, W.X., Li, Z.X., Liu, Y., Yang, Y.H., Liang, X.R., Tu, X.L., 2008. The Bikou basalts in northwestern Yangtze Block, South China: remains of 820-810 Ma continental flood basalts?. *Geological Society of America Bulletin* 120,1478-1492.

Wang, Y. J., Zhang, A. M., Cawood, P. A., Fana, W. M., Xu, J. F., Zhang, G. W., Zhang, Y. Z., 2013. Geochronological, geochemical and Nd-Hf-Os isotopic fingerprinting of an early Neoproterozoic arc-back-arc system in South China and its accretionary assembly along the margin of Rodinia. *Precambrian Research* 231, 343-371.

Whalen, J. B., Currie, K. L., Chappell, B. W., 1987. A-type granites: geochemical characteristics, discrimination and petrogenesis. *Contributions to Mineralogy Petrology* 95,407-419.

Wiedenbeck, M., Alle, P., Corfu, F., Griffin, W. L., Meier, M., Oberli, F., Von Quadt, A., Roddick, J. C., Spiegel, W., 1995. Three natural zircon standards for U-Th-Pb, Lu-Hf, trace element and REE analyses. *Geostandards News letter* 19(1): 1-23.

White, A. J. R., Chappell B W. 1977. Ultrametamorphism and granitoid genesis. *Tectonophysics* 43: 7-22.

Wood, D. A., 1980. The application of a Th-Hf-Ta diagram to problems of tectonomagmatic classification and to establishing the nature of crustal contamination of basalitic lavas of the British Tertiary volcanic province. *Earth and Planetary Science Letters* 50, 11-30.

Xiao, L., Zhang, H. F., Ni, P. Z., Xiang, H., Liu, X. M., 2007. LA-ICP-MS U-Pb zircon geochronology of early Neoproterozoic mafic-intermediat intrusions from NW margin of the Yangtze Block, South China: Implication for tectonic evolution. *Precambrian Research* 154, 221-235.

Zhang, G. W., Dong, Y. P., Lai, S. G., Guo, A. L., Meng, Q. R., Liu, S. F., Cheng, S. Y., Yao, A. P., Zhang, Z. Q., Pei, X. Z., Li, S. Z., 2004.Mianlüe tectonic zone and Mianlüe suture zone on southern margin of Qinling-Dabie orogenic belt. *Science in China：Earth Sciences* 47 (4), 300-316.

Zhang, G. W., Guo, A. L., Wang, Y. J., Li, S. Z., Dong, Y. P., Liu, S. F., He, D. F., Cheng, S.Y., Lu, R. K., Yao, A. P., 2013a. Tectonics of South China Continent and its implications. *Science in China: Earth Sciences* 56(11): 1804-1828.

Zhang, J. L., 2008. The Sr-Nd-Pb isotopic geochemistry of Kongling high-grade terrain of the Yangtze craton (South China) and its tectonic implications. *Master's thesis at China University of Geosciences*.

Zhang, S. B., Zheng, Y. F., Zhao, Z. F., Wu, Y. B., Yuan, H. L., Wu, F. Y., 2009. Origin of TTG-like rocks from anatexis of ancient lower crust: Geochemical evidence from Neoproterozoic granitoids in South China. *Lithos*,113, 347-368.

Zhang, S. B., Zheng, Y. F., 2013b. Formation and evolution of Precambrian continental lithosphere in South China. *Gondwana Research* 23,1241-1260.

Zhang, Y.Z., Wang, Y.J., Fan, W.M., Zhang, A.M., Ma, L.Y., 2012. Geochronologicaland geochemical constraints on the metasomatised source for the neopro-terozoic (~825 Ma) high-mg volcanic rocks from the Cangshuipu area (HunanProvince) along the Jiangnan domain and their tectonic implications. Precambrian Research 220–221, 139–157.

Zhang, Y.Z., Wang, Y.J., Geng, H.Y., Zhang, Y.H., Fan, W.M., Zhong, H., 2013c. Early neoproterozoic (~850 Ma) back-arc basin in the Central Jiangnan Orogen (Eastern South China): Geochronological and petrogenetic constraints frommeta-basalts. Precambrian Research 231, 325–342.

Zhang, Y.Z., Wang, Y.J., Zhang,Y. H, Zhang, A.M., 2015. Neoproterozoic assembly of the Yangtze and Cathaysia blocks: Evidence from the Cangshuipu Group and associated rocks along theCentral Jiangnan Orogen, South China. Precambrian Research 269, 18–30.

Zhao, G. C., Cawood, P. A., 2012. Precambrian geology of China. *Precambrian Research* 222-223, 13-54.

Zhao, J. H., Zhou, M. F., 2007. Geochemistry of Neoproterozoic mafic intrusions in the Panzhihua district (Sichuan Province, SW China): Implications for subduction-related metasomatism in the upper mantle. *Precambrian Research* 152，27-47.

Zhao, J. H., Zhou, M. F., 2008. Neoproterozoic adakitic plutons in the northern margin of the Yangtze Block, China: Partial melting of a thickened lower crust and implications for secular crustal evolution. *Lithos* 104, 231-248

Zhao, J. H., Zhou, M. F., 2009a. Melting of newly formed mafic crust for the formation of Neoproterozoic I-type granite in the Hannan region, South China. *Journal of Geology* 117(1), 54-70.

Zhao, J. H., Zhou, M.F., 2009b. Secular evolution of the Neoproterozoic lithospheric mantle underneath the northern margin of the Yangtze Block, South China. *Lithos* 107, 152-168.

Zhao, J. H., Zhou, M. F., Zheng, J. P., Fang, S. M., 2010a. Neoproterozoic crustal growth and reworking of the Northwestern Yangtze Block: Constraints from the Xixiang dioritic intrusion, South China. *Lithos*, 120, 439-452.

Zhao, J. H., Zhou, M. F., Zheng, J. P., 2010b. Metasomatic mantle source and crustal contamination for the formation of the Neoproterozoic mafic dike swarm in the northern Yangtze Block, South China. *Lithos* 115, 177-189.

Zhao, J.H., Zhou, M.F., Yan, D.P., Zheng, J.P., Li, J.W., 2011. Reappraisal of the ages of Neoproterozoic strata in South China: no connection with the Grenvillian orogeny. *Geology* 39, 299-302.

Zhao, J.H., Zhou, M. F., Zheng, J. P., 2013a. Neoproterozoic high-K granites produced by melting of newly formed mafic crust in the Huangling region, South China. *Precambrian Research* 233, 93-107.

Zhao, J. H., Zhou, M. F., Zheng, J. P., Griffin, W. L., 2013b. Neoproterozoic tonalite and trondhjemite in the huangling complex, south china: crustal growth and reworking in a continental arc environment. *American Journal of Science* 313, 540-583.

Zhou, M. F., Kennedy, A.K., Sun, M., Malpas, J., Lesher, C.M., 2002. Neoproterozoic arc-related mafic intrusions in the northern margin of South China: implications for accretion of Rodinia. *Journal of Geology* 110, 611-618.

Zhou, M. F., Ma, Y. X., Yan, D. P., Xia, X. P., Zhao, J. H., Sun, M., 2006. The Yanbian Terrane (Southern Sichuan Province, SW China): A Neoproterozoic arc assemblage in the western margin of the Yangtze Block. *Precambrian Research* 144: 19-38.

Zheng, Y. F., Zhang, S. B., Zhao, Z. F., Wu, Y. B., Li, X. H., Li, Z. X., Wu, F. Y., 2007. Contrasting zircon Hf and O isotopes in the two episodes of Neoproterozoic granitoids in South China: Implications for growth and

reworking of continental crust. *Lithos* 96, 127-150.
Zheng, Y. F., Wu, R. X., Wu, Y. B., Zhang, S. B., Yuan, H. L., Wu, F.Y., 2008. Rift melting of juvenile arc-derived crust: Geochemical evidence from Neoproterozoic volcanic and granitic rocks in the Jiangnan Orogen, South China. *Precambrian Research* 163, 351-383.

Figure captions

Fig.1. (a) Tectonic sketch showing tectonic position of the study area. (b) Simplified structural map showing the Sanligang-Sanyang fault and surrounding units of the Tongbai orogen. (c) Simplified geological map of the Sanligang region, northern margin of the Yangtze Block (modified after HBBGMR (1982)).

Fig.2. Field photos of the Sanligang mafic dikes and granitoids from SSFB, northern margin of the Yangtze Block. (a) Mafic dike (diabase), (b) and (c) the Huashan Groups were generally intruded by the Sanligang granitoid, (d) quartz diorite, (e) the pelitic xenoliths, and (f) the mafic enclaves in the pluton.

Mineral abbreviations: Aug: Augite; Hb: hornblende; Pl: plagioclase; Qtz: quartz.

Fig.3. Photomicrographs showing texture and mineral assemblages of the Sanligang mafic dikes and granitoids from SSFB, northern margin of the Yangtze Block. (a) Mafic dike (diabase, X23), (b) quartz diorite (S09), (c) granodiorite (S10), (d) granodiorite (S04), (e) granodiorite (S04), and (f) granodiorite (S06).Mineral abbreviations: Aug: Augite; Ep: Epidote; Hb: hornblende; Mag: Magnetite; Pl: plagioclase; Qtz: quartz; Ser: Sericite.

Fig.4. Zircon U-Pb Concordia diagrams for the Sanligang mafic dike (a) and granitoids (b-d) from SSFB, northern margin of the Yangtze Block. Cathodoluminescence (CL) images for representative zircon grains showing internal structures, analytical locations, apparent $^{206}Pb/^{238}U$ ages (Ma, red number) and $\varepsilon_{Hf}(t)$ values (yellow number). The scale bars in the CL images are 50 μm.

Fig.5. Geochemical classification of the Sanligang granitoids from the SSFB, northern margin of the Yangtze Block. (a) SiO_2 vs. K_2O+Na_2O-CaO, (b) A/CNK vs. A/NK, (c) SiO_2 vs. TFeO/(TFeO+MgO), and (d) SiO_2 vs. K_2O+ Na_2O. Xixiang diorites, Huangling granites, tonalites and trondhjemites are from

Zhao et al.(2010a, 2013a and 2013b).

Fig.6. Harker diagrams illustrating major element of Sanligang mafic dikes and granitoids from SSFB, northern margin of the Yangtze Block. The background references fields of (b) and (e) are from Jung et al. (2002) and references therein.

Fig.7. Chondrite-normalized REE patterns and Primitive mantle-normalized trace element spider diagrams for Sanligang mafic dikes and granitoids from SSFB, northern margin of the Yangtze Block. The values of OIB, E-MORB, N-MORB and Normalizing values are from Sun and McDonough (1989), Barren Island island arc basalts are from Andaman arc in the northeastern Indian Ocean (Luhr and Haldar, 2006). Xixiang diorite and Huangling granite are from Zhao et al.(2010a, 2013a).

Fig.8. Histograms of $\varepsilon_{Hf}(t)$ values and single-stage Hf model ages (T_{DM1}) for zircon from the Sanligang mafic dikes and granitoids from SSFB, northern margin of the Yangtze Block.

Fig.9. (a) $\varepsilon_{Hf}(t)$ values corrected to the crystallization ages of zircons for the Sanligang mafic dikes and granitoids from SSFB, northern margin of the Yangtze Block. Reference lines representing meteoritic Hf evolution (CHUR) and depleted mantle are from Blichert-Toft and Albarede (1997) and Griffin et al. (2006), respectively. (b) Plot of $\varepsilon_{Nd}(t)$ vs. $^{87}Sr/^{86}Sr(i)$ for the Sanligang mafic dikes and granitoids. The Hannan mafic intrusions (Zhao and Zhou, 2009b), Hannan adakitic rocks (Zhao and Zhou, 2008), Tianpinghe granits (Zhao and Zhou, 2009a) and Xixiang diorites (Zhao et al., 2010a) are from the Hannan region, northwestern margin of the Yangtze Block. The Huangling mafic dikes (Zhao et al., 2010b), granites (Zhao et al., 2013a), Huangling tonalites-trondhjemites (Zhao et al., 2013b) and TTG-like rocks (Zhang et al., 2009) are from the Huangling dome, Central Yangtze Block. The Hf-Nd isotope comparison of the Kongling metamorphic complex datas from Gao et al. (1999) and Zhang et al. (2008).

Fig. 10. Tectonic discriminant diagrams for Sanligang mafic dikes and granitoids from SSFB, northern margin of the Yangtze Block. (a) Nb-Zr-Y diagram (after Meschede, 1986). (A1) within-plate alkali basalts, (A2) within-plate alkali basalts and within-plate tholeiites, (B) E-MORB, (C) within-plate

tholeiites and volcanic-arc basalts, (D) N-MORB and volcanic-arc basalts. (b) Hf-Th-Nb diagram (after Wood, 1980); (c) La/Nb vs. Ba/Nb (after Fan et al., 2004); La/Nb vs. Nb/Th (after Fan et al., 2004); (e) Nb/Yb vs. Th/Yb (after Dilek and Furnes, 2011); (f) Ta/Yb vs. Th/Yb (after Pearce, 1983), The Mariana arc regions defined by Elliot et al. (1997). (g) Yb vs. Ta (after Pearce et al., 1984), (h) Yb + Ta vs. Rb (after Pearce et al., 1984).

Fig.11. Plots of (a) Sr/Y vs. Y (Defant and Drummond, 1990), (b) $(La/Yb)_N$ vs. Yb_N (Martin, 1999) , (c) Th/Tb vs. Th/Ta and (d) Mg# versus SiO_2 for the Sanligang granitoids. The Huangling Neoproterozoic intrusions are from Zhao et al. (2010b; 2013b) in the plot of (c). The reference fields for mantle melts, high Mg andesites, hybridised melts, sanukitoid and experimental melts under 1–4 GPa are from Souza et al. (2007) and references therein in the plot (d).

Fig.12. Geological map of the Yangtze Block showing the distribution of the Neoproterozoic rocks (modified after Zhao and Cawood(2012) and Bader et al. (2013)).

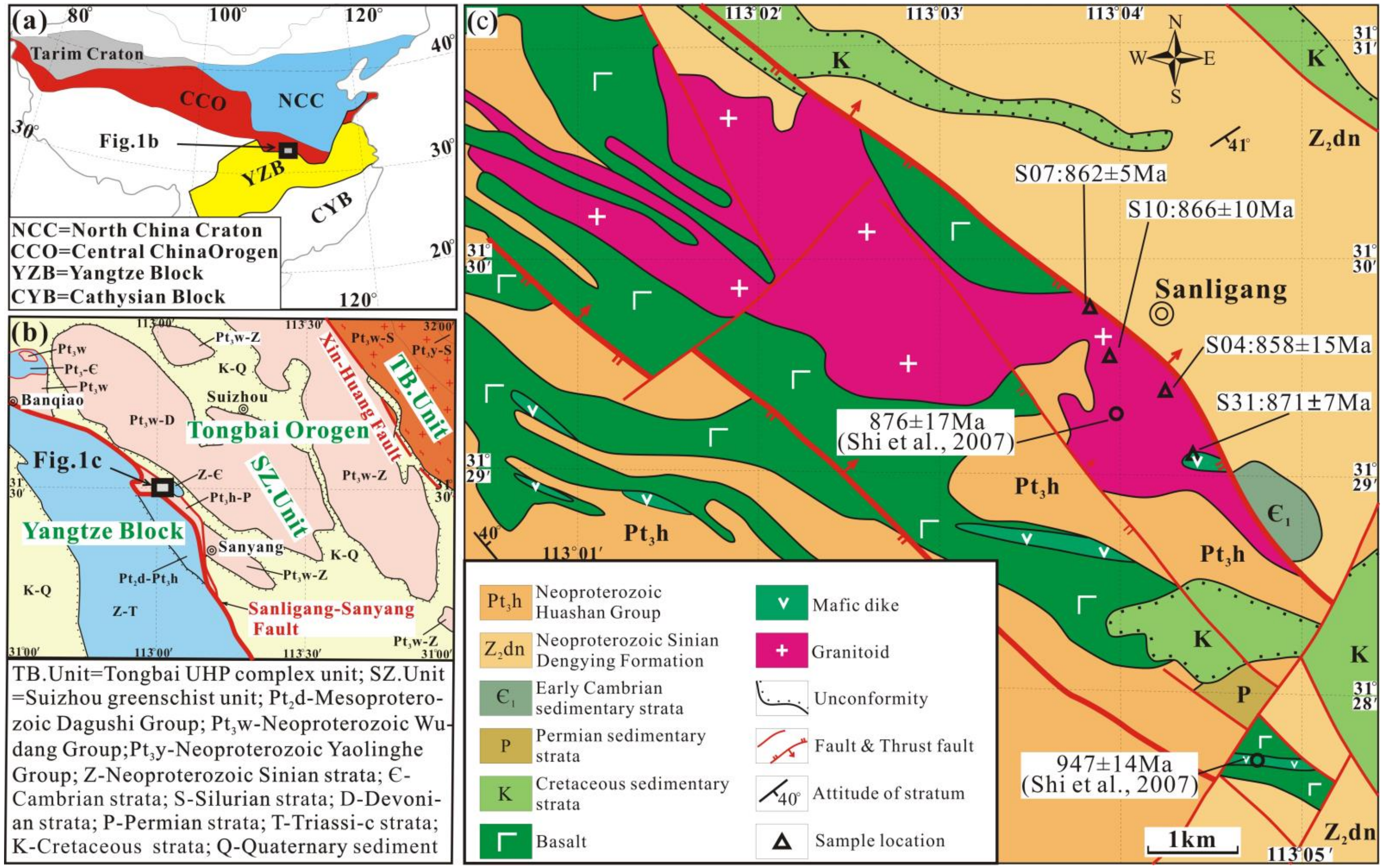

Figure.1 (a) Tectonic sketch showing tectonic position of the study area. (b) Simplified structural map showing the Sanligang-Sanyang fault and surrounding units of the Tongbai orogen. (c) Simplified geological map of the Sanligang region, northern margin of the Yangtze Block (modified after HBBGMR (1982)).

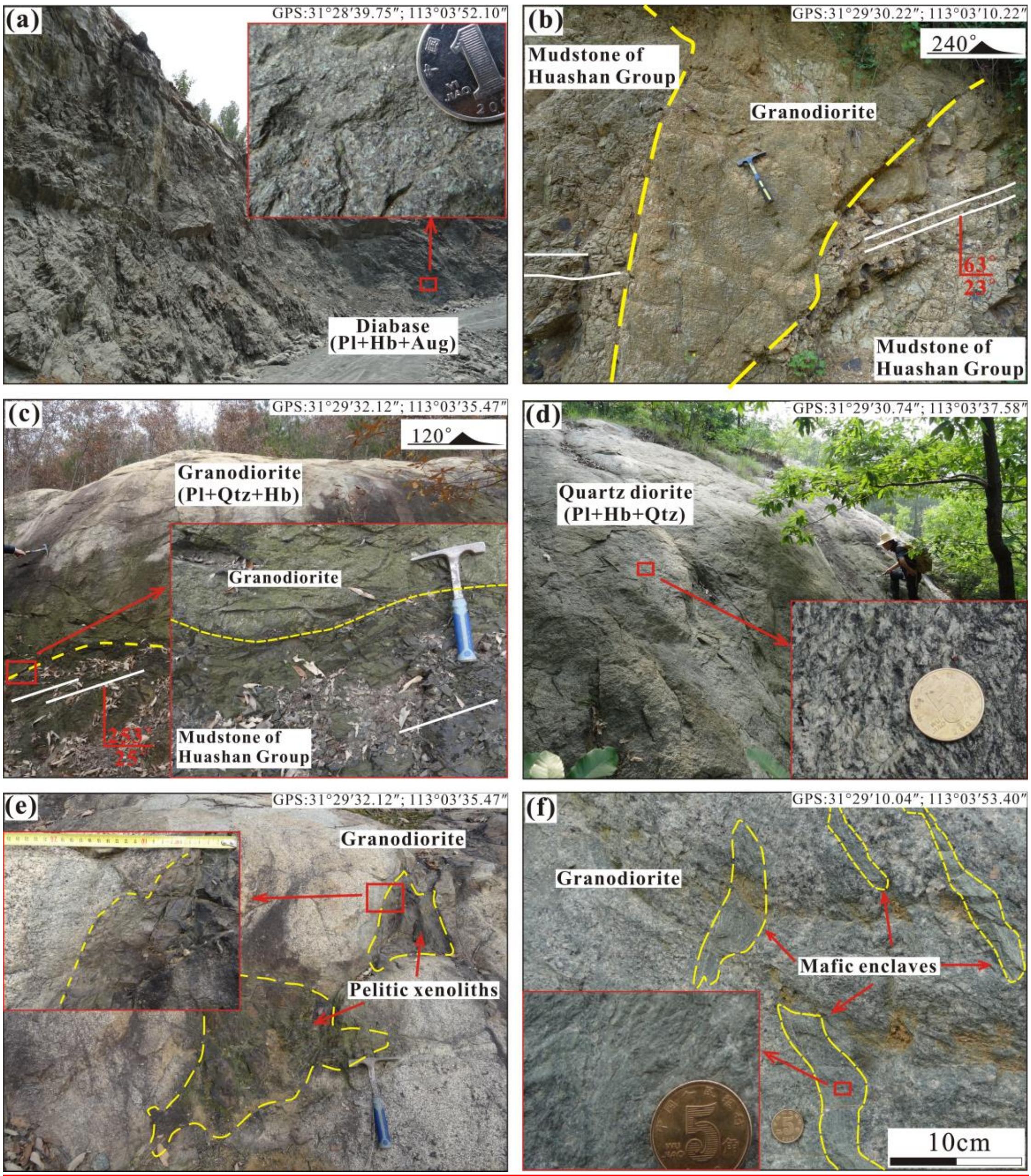

Figure.2 Field photos of the Sanligang mafic dikes and granitoids from SSFB, northern margin of the Yangtze Block. (a) Mafic dike (diabase), (b) and (c) the Huashan Groups were generally intruded by the Sanligang granitoid, (d) quartz diorite, (e) the politic xenoliths, and (f) the mafic enclaves in the pluton.

Mineral abbreviations: Aug: Augite; Hb: hornblende; Pl: plagioclase; Qtz: quartz.

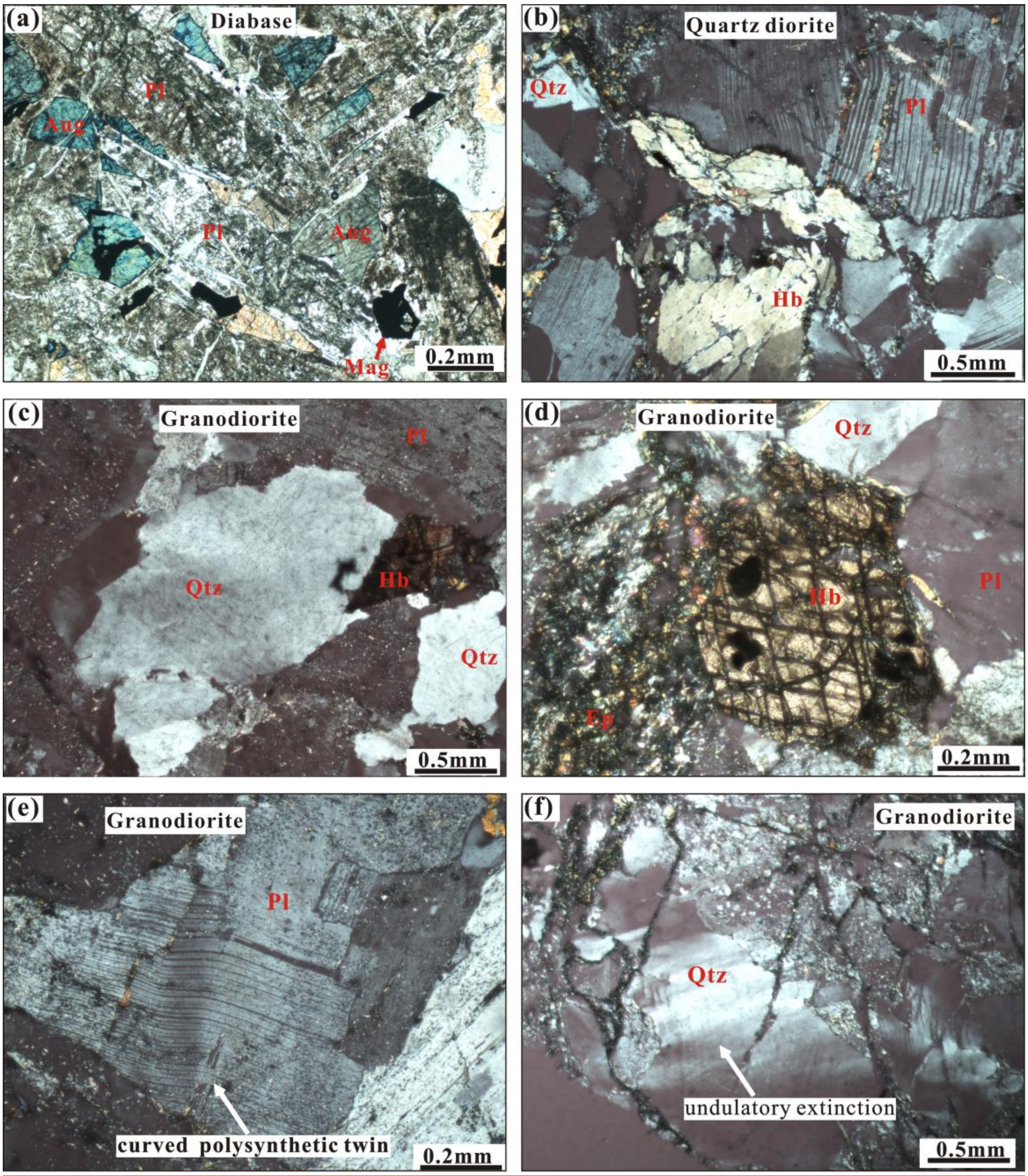

Figure.3 Photomicrographs showing texture and mineral assemblages of the Sanligang mafic dikes and granitoids from SSFB, northern margin of the Yangtze Block. (a) Mafic dike (diabase, X23), (b) quartz diorite (S09), (c) granodiorite (S10), (d) granodiorite (S04), (e) granodiorite (S04), and (f) granodiorite (S06).

Mineral abbreviations: Aug: Augite; Ep: Epidote; Hb: hornblende; Mag: Magnetite; Pl: plagioclase; Qtz: quartz; Ser: Sericite.

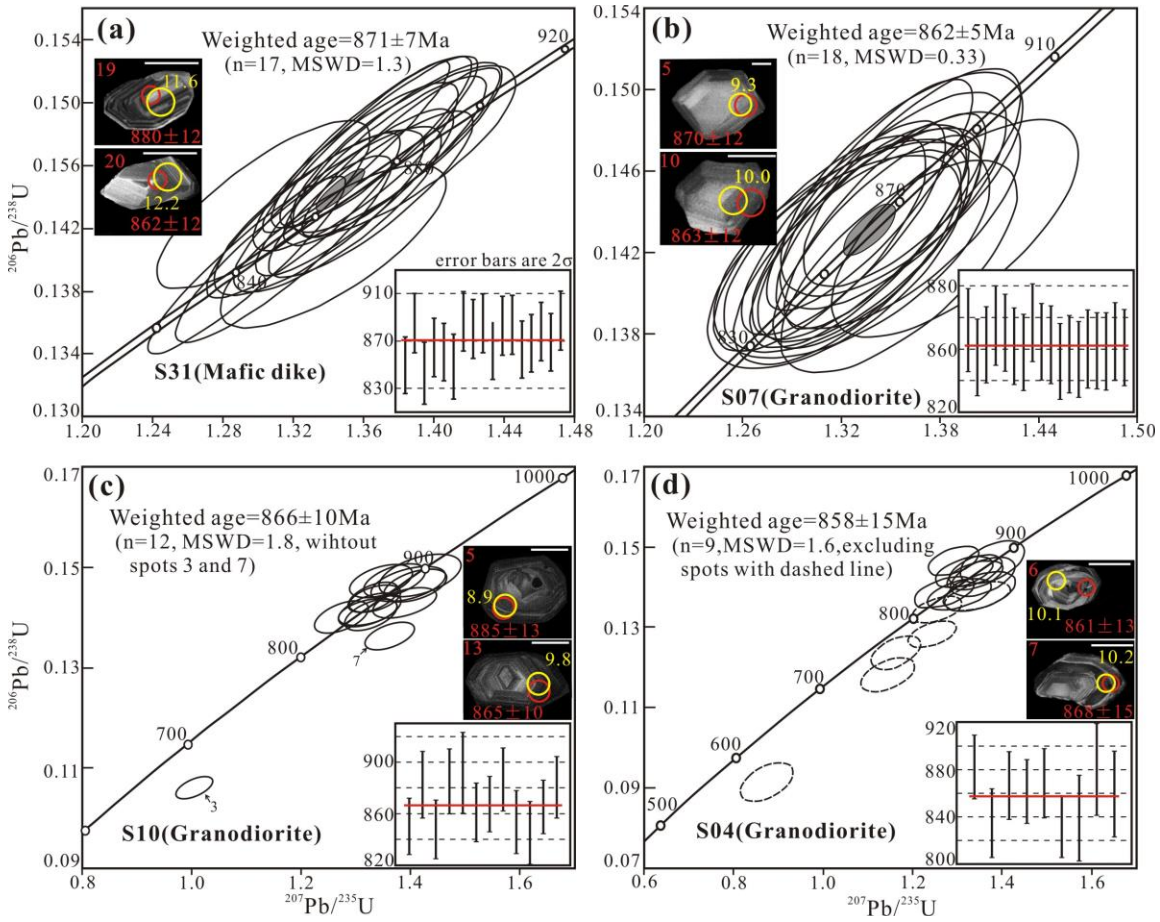

Figure.4 Zircon U-Pb Concordia diagrams for the Sanligang mafic dike (a) and granitoids (b-d) from SSFB, northern margin of the Yangtze Block. Cathodoluminescence (CL) images for representative zircon grains showing internal structures, analytical locations, apparent $^{206}Pb/^{238}U$ ages (Ma, red number) and $\varepsilon_{Hf}(t)$ values (yellow number). The scale bars in the CL images are 50 μm.

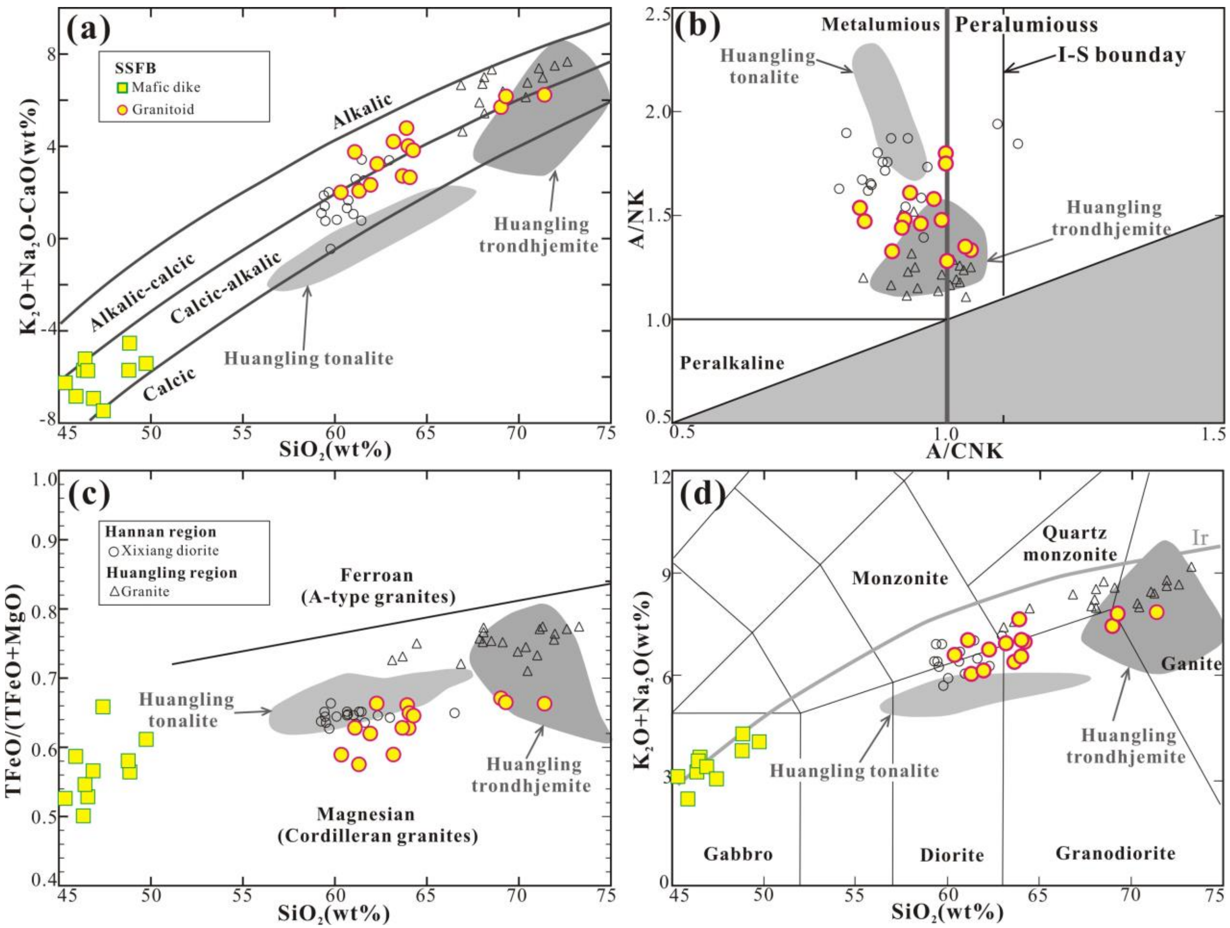

Figure.5 Geochemical classification of the Sanligang granitoids from the SSFB, northern margin of the Yangtze Block. (a) SiO_2 vs. K_2O+Na_2O-CaO, (b) A/CNK vs. A/NK, (c) SiO_2 vs. TFeO/(TFeO+MgO), and (d) SiO_2 vs. $K_2O+ Na_2O$. Xixiang diorites, Huangling granites, tonalites and trondhjemites are from Zhao et al.(2010a, 2013a and 2013b).

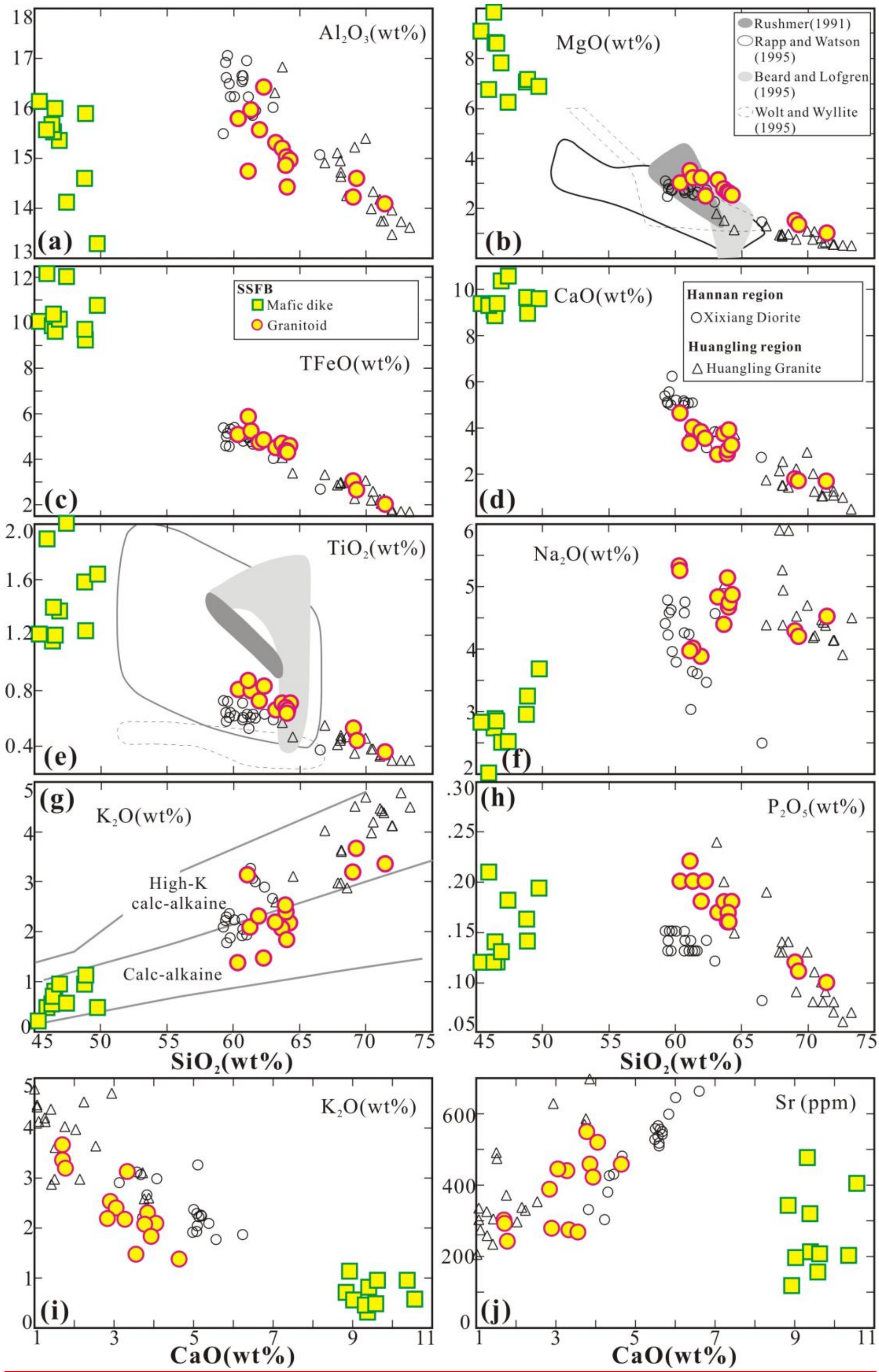

Figure.6 Harker diagrams illustrating major element of Sanligang mafic dikes and granitoids from SSFB, northern margin of the Yangtze Block. The background references fields of (b) and (e) are from Jung et al. (2002) and references therein.

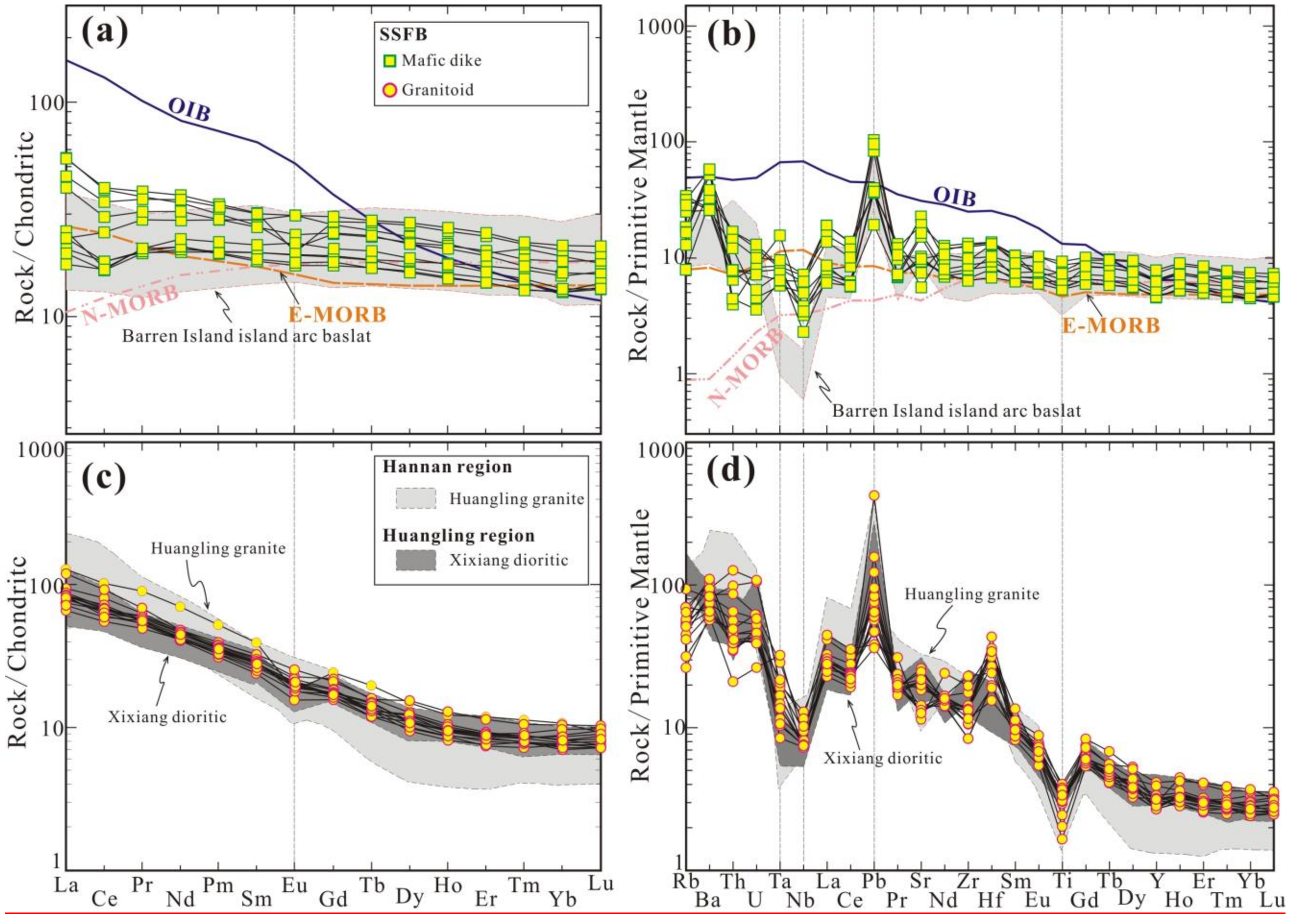

Figure.7 Chondrite-normalized REE patterns and Primitive mantle-normalized trace element spider diagrams for Sanligang mafic dikes and granitoids from SSFB, northern margin of the Yangtze Block. The values of OIB, E-MORB, N-MORB and Normalizing values are from Sun and McDonough (1989), Barren Island island arc basalts are from Andaman arc in the northeastern Indian Ocean (Luhr and Haldar, 2006). Xixiang diorite and Huangling granite are from Zhao et al.(2010a, 2013a).

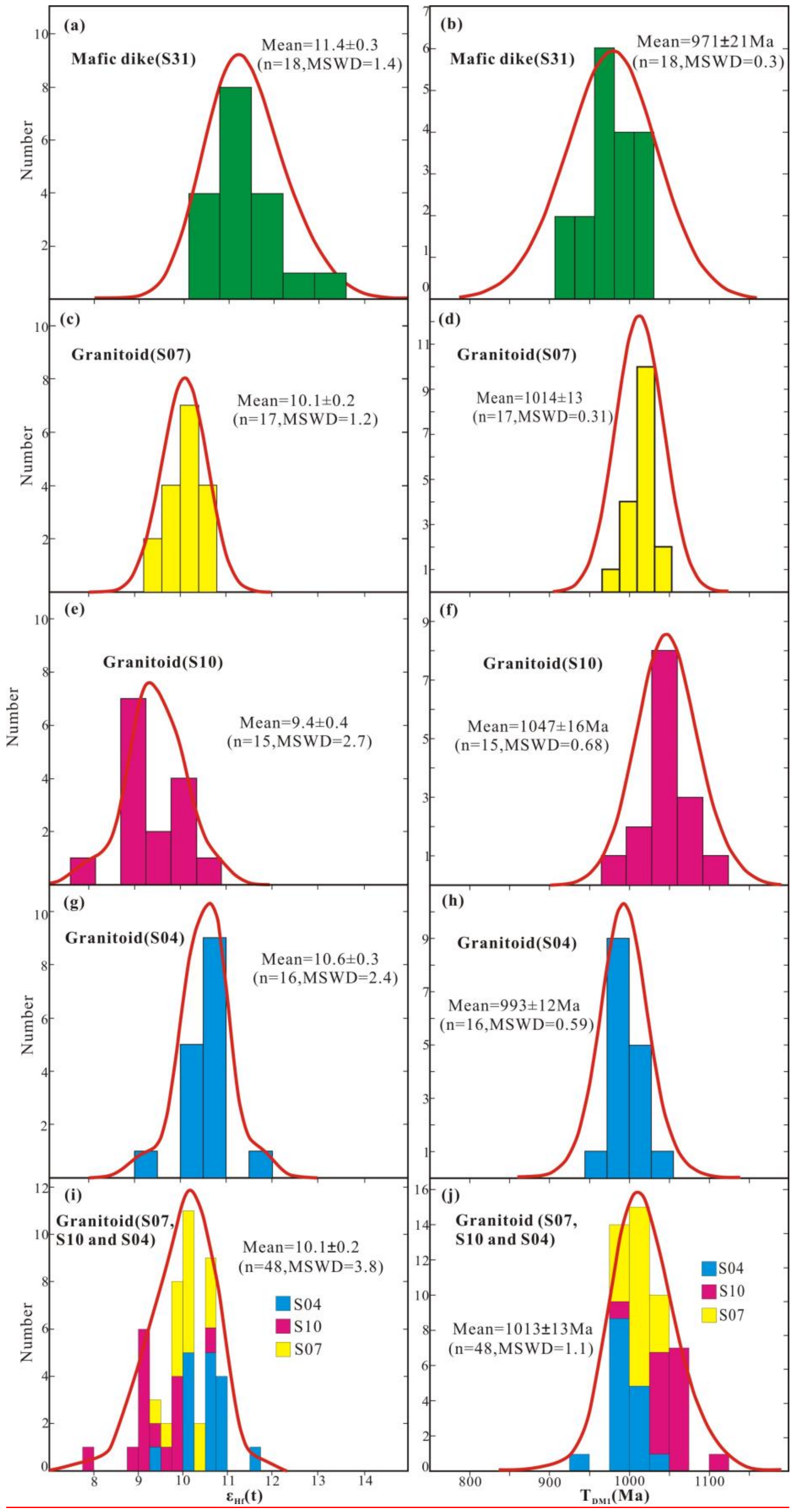

Figure.8 Histograms of ε_{Hf}(t) values and single-stage Hf model ages (T_{DM1}) for zircon from the Sanligang mafic dikes and granitoids from SSFB, northern margin of the Yangtze Block.

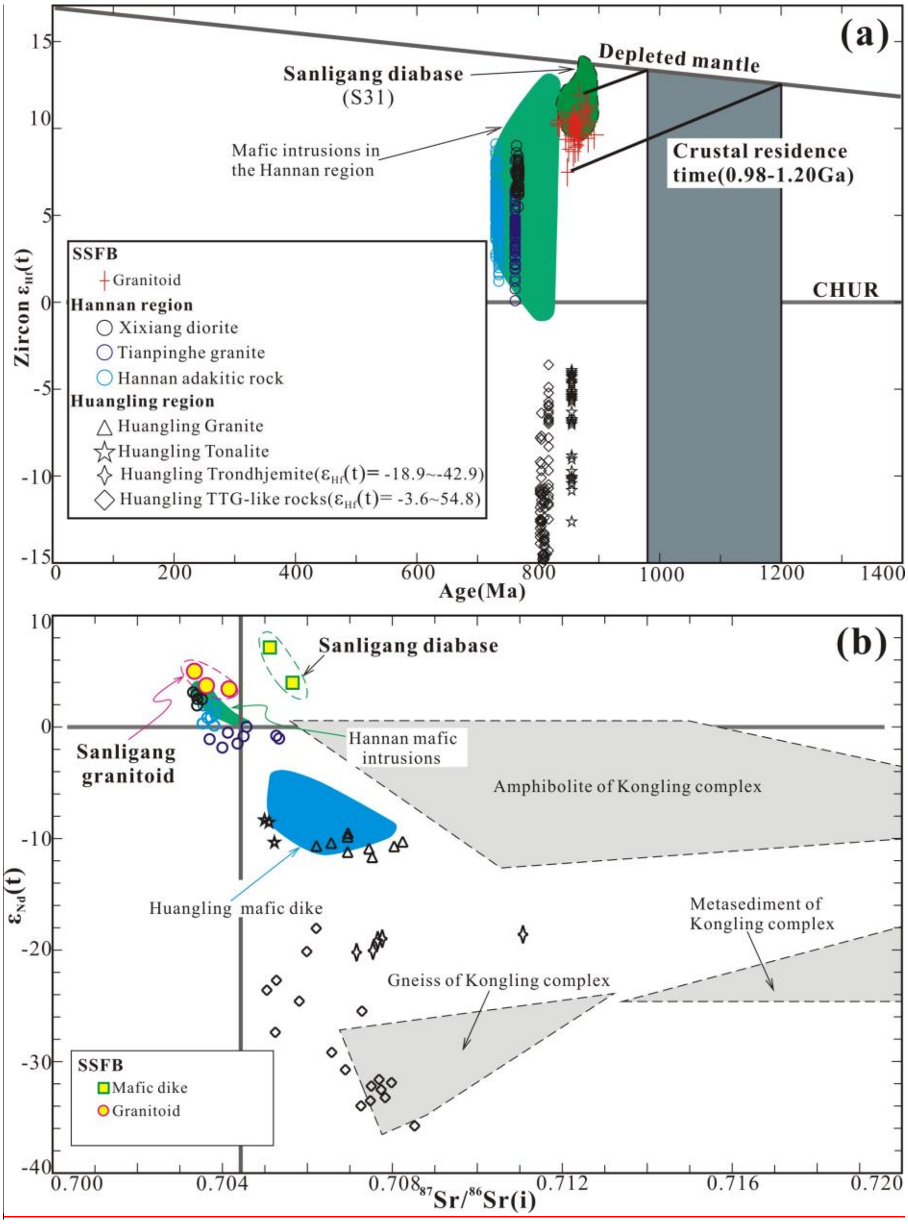

Figure.9 (a) $\varepsilon_{Hf}(t)$ values corrected to the crystallization ages of zircons for the Sanligang mafic dikes and granitoids from SSFB, northern margin of the Yangtze Block. Reference lines representing meteoritic Hf evolution (CHUR) and depleted mantle are from Blichert-Toft and Albarede (1997) and Griffin et al. (2006), respectively. (b) Plot of $\varepsilon_{Nd}(t)$ vs. $^{87}Sr/^{86}Sr(i)$ for the Sanligang mafic dikes and granitoids. The Hannan mafic intrusions (Zhao and Zhou, 2009b), Hannan adakitic rocks (Zhao and Zhou, 2008), Tianpinghe granits (Zhao and Zhou, 2009a) and Xixiang diorites (Zhao et al., 2010a) are from the Hannan region, northwestern margin of the Yangtze Block. The Huangling mafic dikes (Zhao et al., 2010b), granites (Zhao et al., 2013a), Huangling tonalites-trondhjemites (Zhao et al., 2013b) and TTG-like rocks (Zhang et al., 2009) are from the Huangling dome, Central Yangtze Block. The Hf-Nd isotope comparison of the Kongling metamorphic complex datas from Gao et al. (1999) and Zhang et al. (2008).

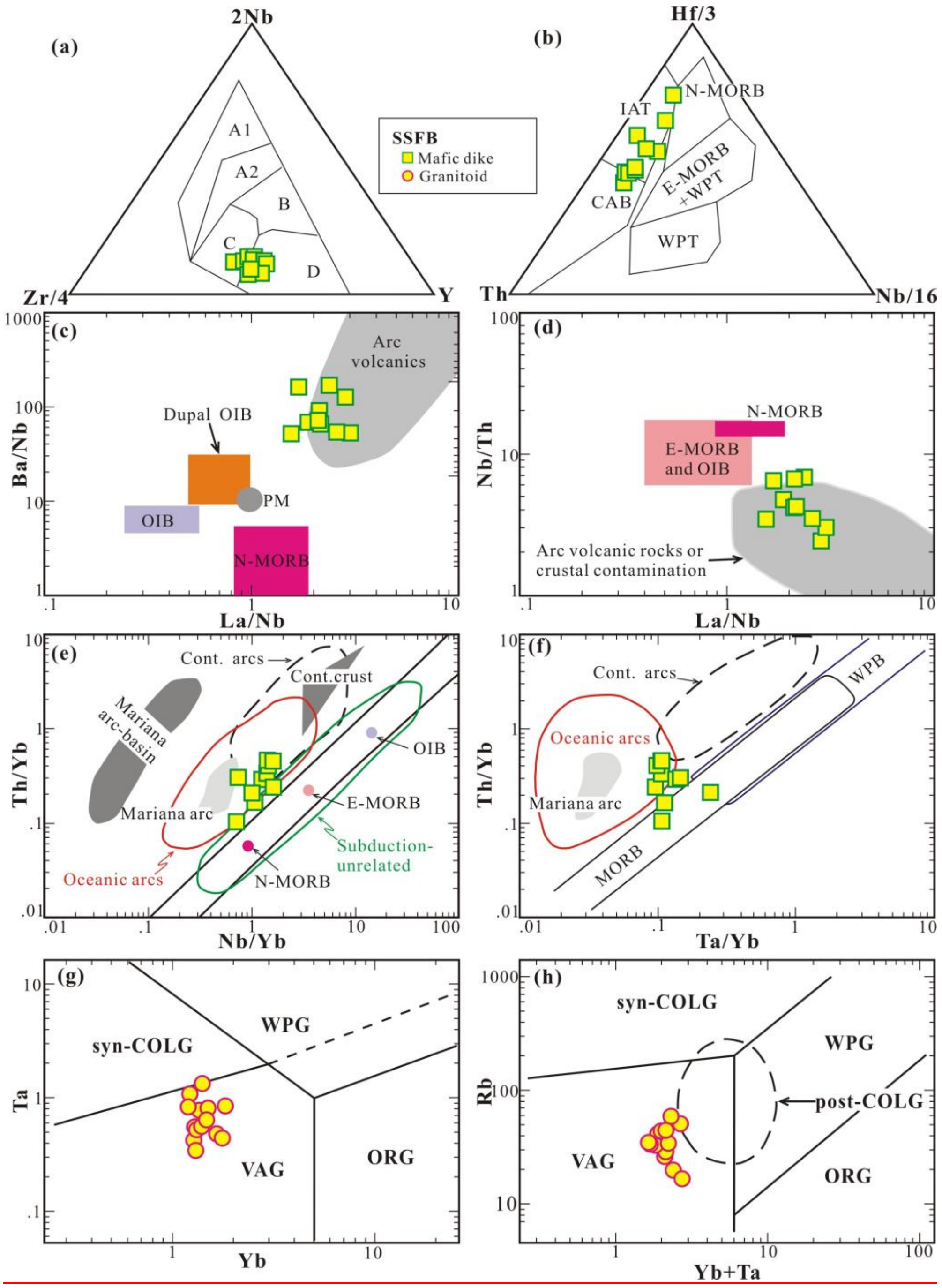

Figure.10 Tectonic discriminant diagrams for Sanligang mafic dikes and granitoids from SSFB, northern margin of the Yangtze Block. (a) Nb-Zr-Y diagram (after Meschede, 1986). (A1) within-plate alkali basalts, (A2) within-plate alkali basalts and within-plate tholeiites, (B) E-MORB, (C) within-plate tholeiites and volcanic-arc basalts, (D) N-MORB and volcanic-arc basalts. (b) Hf-Th-Nb diagram (after Wood, 1980); (c) La/Nb vs. Ba/Nb (after Fan et al., 2004); La/Nb vs. Nb/Th (after Fan et al., 2004); (e) Nb/Yb vs. Th/Yb (after Dilek and Furnes, 2011); (f) Ta/Yb vs. Th/Yb (after Pearce, 1983), The Mariana arc regions defined by Elliot et al. (1997). (g) Yb vs. Ta (after Pearce et al., 1984), (h) Yb + Ta vs. Rb (after Pearce et al., 1984).

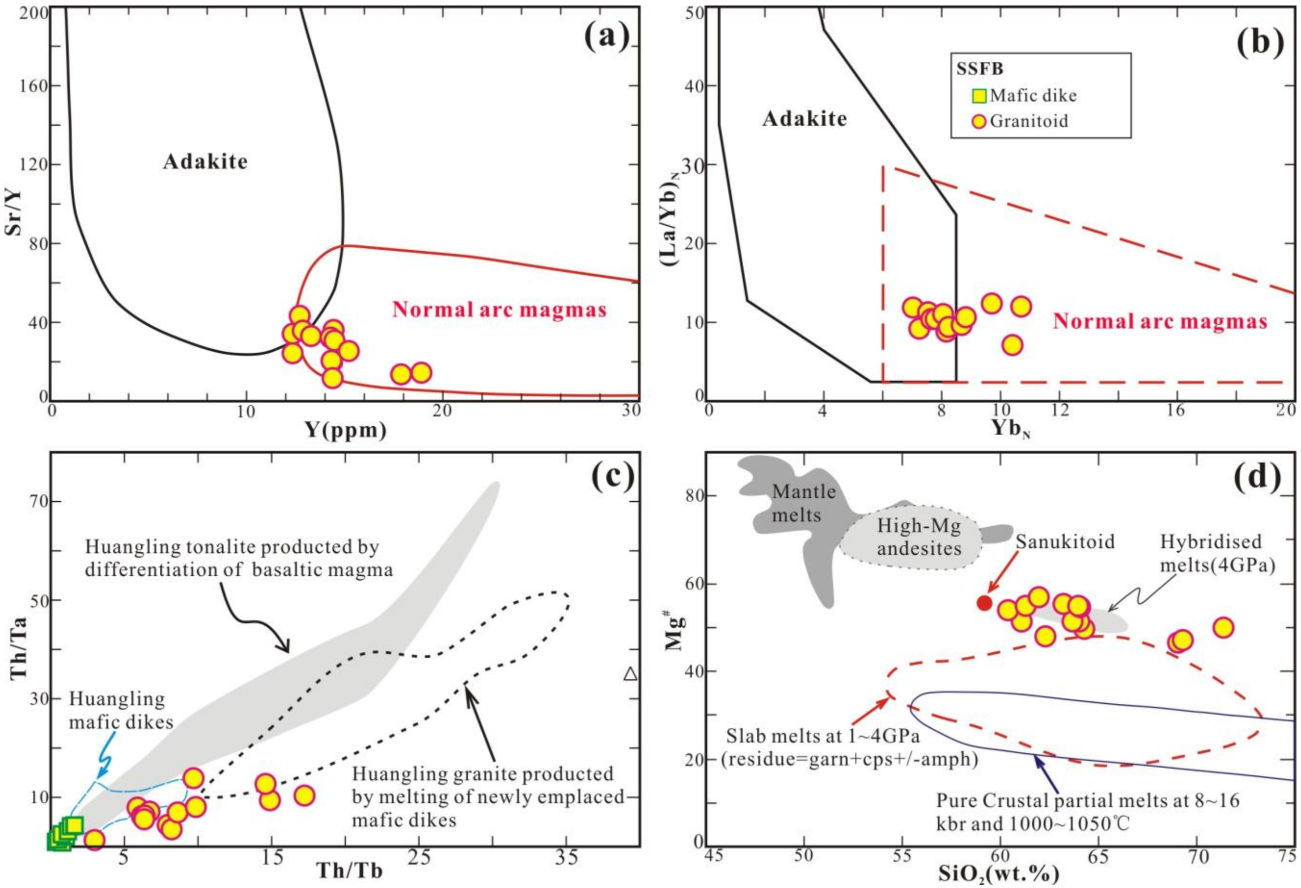

Figure.11 Plots of (a) Sr/Y vs. Y (Defant and Drummond, 1990), (b) $(La/Yb)_N$ vs. Yb_N (Martin, 1999) , (c) Th/Tb vs. Th/Ta and (d) Mg# versus SiO_2 for the Sanligang granitoids. The Huangling Neoproterozoic intrusions are from Zhao et al. (2010b; 2013b) in the plot of (c). The reference fields for mantle melts, high Mg andesites, hybridised melts, sanukitoid and experimental melts under 1–4 GPa are from Souza et al. (2007) and references therein in the plot (d).

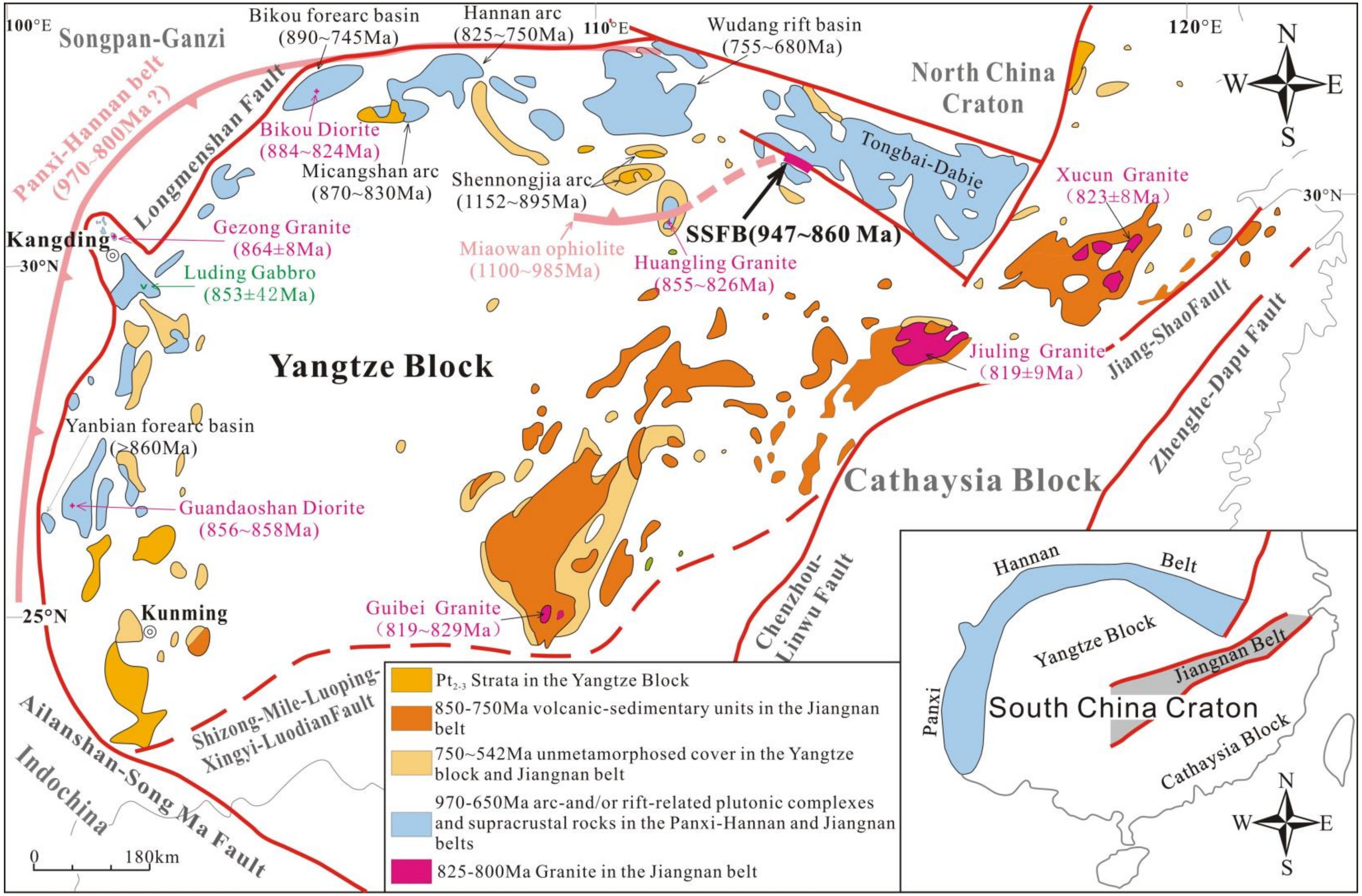

Figure.12 Geological map of the Yangtze Block showing the distribution of the Neoproterozoic rocks (modified after Zhao and Cawood(2012) and Bader et al. (2013)).